공 학 박 사 학 위 논 문

Improvement of Electrochlorination Efficiency using Oxygen-Evolution-Suppressing Anodes in Dilute Chloride Solutions

저농도 Cl^-용액에서 염소발생효율 향상을 위한 산소발생억제 전극 이용

2021년 8월

서울대학교 대학원

화학생물공학부

김 성 수

Improvement of Electrochlorination Efficiency using Oxygen-Evolution-Suppressing Anodes in Dilute Chloride Solutions

by

Seongsoo Kim

under the supervision of

Professor Changha Lee, Ph. D.

A dissertation submitted in partial fulfillment of

the requirements for the Degree of

Doctor of Philosophy

August 2021

SCHOOL OF CHEMICAL AND BIOLOGICAL ENGINEERING

SEOUL NATIONAL UNIVERSITY

Improvement of Electrochlorination Efficiency using Oxygen-Evolution-Suppressing Anodes in Dilute Chloride Solutions

저농도 Cl^-용액에서 염소발생효율 향상을 위한 산소발생억제 전극 이용

지도교수 이 창 하

이 논문을 공학박사 학위논문으로 제출함

2021년 8월

서울대학교 대학원

공과대학 화학생물공학부

김 성 수

김성수의 공학박사 학위논문을 인준함

2021년 8월

위 원 장 _____

부 위 원 장 _____

위 원 _____

위 원 _____

위 원 _____

Abstract

In this study, the IrO_y·FeO_z and IrO_a·CoO_b anodes were fabricated to improve the current efficiency of chlorine evolution reaction (CER) in dilute chloride solutions by lowering the activity of oxygen evolution reaction (OER). Dimensionally stable anodes (DSAs) are regarded to be optimized electrodes for electrochlorination owing to their excellent electrocatalytic activity for the CER and reliable stability. However, in dilute chloride solutions, DSAs preferentially produce oxygen rather than chlorine because of their low overpotential for OER. Considering the frequent use of electrochlorination in dilute conditions, the poor efficiency of DSAs severely limits their environmental and industrial applications. Although there are several attempts to maintain a high concentration of chloride such as a continuous supply of synthesized brine or seawater, these require additional facilities and costs. Furthermore, in consideration of the global trend of a small-scaled, decentralized water treatment system, electrochlorination in dilute conditions becomes increasingly important. Therefore, this study aims to improve the electrochlorination efficiency in dilute chloride solutions by suppressing the competitive reaction of CER, i.e. OER.

Herein, iron oxide and cobalt oxide were used as an OER-suppressing catalyst to improve the CER efficiency of DSAs in dilute chloride solutions. Iron oxide (FeO_x) is well-known to have an extremely slow reaction rate of OER with a high OER

overpotential. Meanwhile, cobalt oxide (Co_3O_4) was reported to have a much higher working potential for OER than that for CER, which can be interpreted as Co_3O_4 has high selectivity for CER against OER. Furthermore, Co_3O_4 showed a relatively larger difference in the working potential between the OER and CER compared with other metal oxides. These characteristics of FeO_x and Co_3O_4 can be an indication that they have the potential to improve the CER efficiency in dilute chloride solutions. Although there have been many trials to develop novel anodes with various transition metals, the lifetime of the anodes was too short. Therefore, a small amount of IrO_2 was used as a co-catalyst to enhance the stability of FeO_x and Co_3O_4, resulting in the $IrO_y{\cdot}FeO_z$ and $IrO_a{\cdot}CoO_b$ anodes fabricated by the thermal decomposition method. The $IrO_y{\cdot}FeO_z$ and $IrO_a{\cdot}CoO_b$ showed superior CER efficiency than DSAs not only in dilute chloride solutions but also in concentrated solutions (1 mM − 2000 mM). The improvement in CER efficiency of the anodes is attributed to the synergistic effect of suppressed OER (FeO_x and Co_3O_4) and high CER activity of IrO_2. The stability of the anodes also exceedingly improved compared with that of pristine FeO_x and Co_3O_4. In addition, hazardous byproducts formation during eletrochlorination such as ClO_2^-, ClO_3^-, and ClO_4^- was also examined and confirmed to satisfy the standard for drinking water.

These results suggest that the $IrO_y{\cdot}FeO_z$ and $IrO_a{\cdot}CoO_b$ have great potential to expand the scope of application of the electrochlorination system, particularly in dilute solutions.

Keywords: Iron oxide; Cobalt oxide; Chlorine evolution reaction; Oxygen evolution reaction; Electrochlorination

Student number: 2017-33653

CONTENTS

List of Figures

List of Tables

Chapter 1. Introduction

1.1. Research Background

Water chlorination is the essential part of water treatment which is the process of injecting chlorine (Cl_2) into water to kill microorganisms, bacteria, and viruses. The disinfection process with chlorination prevents waterborne diseases such as cholera and typhoid fever. In conventional chlorination, liquefied Cl_2 and sodium hypochlorite solution are used to inject an adequate dose of Cl_2 into water. However, safety concerns arise from the storage and transport of hazardous reagents (Patermarakis and Fountoukidis 1990, Kraft, Stadelmann et al. 1999, Jeong, Kim et al. 2007, Nath, Wang et al. 2011, Choi, Shim et al. 2013, Cotillas, Llanos et al. 2015, Saha and Gupta 2017). To minimize safety problems, electrochlorination is adopted as an alternative to conventional chlorination due to its great merit of on-site Cl_2 production. Electrochlorination is an environmentally friendly, economical, and easily operated system comprised of an anode, cathode, and power supply. Cl_2 is electrochemically produced from the anode by oxidation of chloride (Cl^-). In electrochlorination, the conventional dimensionally stable anodes (DSAs) (generally refer to IrO_2 and RuO_2) has been considered as an optimized electrode because of its outstanding performance in the chlorine evolution reaction (CER) and reliable stability (Trasatti 2000, Malpass, Miwa et al. 2007, Khelifa, Aoudj et al. 2013, Menzel, Ortel et al. 2013, Cotillas, Llanos et al. 2015, Le Luu, Kim et al.

2015, Saha and Gupta 2017). However, in dilute Cl^- solutions, the current efficiency for CER of DSA is significantly decreased due to its low overpotential for oxygen evolution reaction (OER) and Cl^--deficient environment (Kraft, Stadelmann et al. 1999, Neodo, Rosestolato et al. 2012, Grgur and Mijin 2014, Tavakkoli, Kallio et al. 2016, Oakton, Lebedev et al. 2017). In other words, as the concentration of Cl^- decreases, OER which is the competitive reaction of CER becomes dominant. DSAs are also known as excellent electrodes for OER as well as CER. In dilute Cl^- solutions, DSAs preferentially produce oxygen (O_2) rather than Cl_2. Considering most of the water which needs to be treated for use (domestic sewage, groundwater, river, and lake) contains a very low concentration of Cl^-, the poor effectiveness of DSAs in dilute Cl^- solution severely limits environmental and industrial applications of electrochlorination. There have been various approaches to supply concentrated Cl^- solution into electrolyzer via synthesizing saturated Cl^- solution, and mixing of seawater or brine. However, these require additional costs and equipment (electrolytic cell, chemicals, and pump etc.) (Mendia 1982, Patermarakis and Fountoukidis 1990, Khelifa, Moulay et al. 2004, Hooper 2005, Malpass, Miwa et al. 2007). Furthermore, a small-scaled and decentralized water treatment system becomes increasingly important in consideration of the global goals ("Clean Water and Sanitation" is one of the Sustainable Development Goals (SDGs) supported by United Nations). Therefore, it is worthwhile to enhance the current efficiency for CER in dilute Cl^- solutions. The current efficiency for CER strongly depends on

several parameters including the electrode materials, pH, current density, composition of the solution, and temperature. Among them, electrode materials are considered as the most crucial factor. One strategy to improve the CER efficiency is a selection of electrode materials that can suppress the competitive reaction of the CER. In other words, materials whose reaction rate of OER is slow can be electrode candidates for efficient Cl_2 production in dilute Cl^- solution.

Iron oxide can be a good candidate to suppress OER because it has an extremely slow reaction rate of OER with a high OER overpotential (Sivula, Le Formal et al. 2011, Spray, McDonald et al. 2011, Rahman and Joo 2012, Cong, Chen et al. 2014, Fu, Jiang et al. 2014, Yang, Kang et al. 2014, Tamirat, Su et al. 2015, Zeng, Bai et al. 2015, Carroll and Gamelin 2016). In addition, according to the previous study (Trasatti 1984), iron oxide revealed a much higher working potential for OER than that for CER, which can be interpreted as iron oxide has high selectivity for CER against OER. Furthermore, iron oxide showed a relatively larger difference in the working potential between the OER and CER compared with other metal oxides. These characteristics of iron oxide can be an indication that iron oxide has more potential to improve the CER efficiency in dilute Cl^- solutions than other metal oxides. Nevertheless, to the best of our knowledge, iron oxide has not been investigated as an OER suppressor for efficient CER in dilute Cl^- solutions.

Similarly, cobalt oxide exhibited a much higher working potential for OER than

that for CER (Trasatti 1984). Although the overpotential for OER and CER of cobalt oxide was much lower than that of iron oxide, the gap between the working potential for OER and CER was even larger than iron oxide. This indicates cobalt oxide also produces chlorine effectively with low energy consumption compared to iron oxide.

There are many trials to develop electrodes with various transition metals such as Fe, Co, Ni, Mn, and Ti (Hummelgård, Karlsson et al. 2013, Gokuladeepan and Karthigeyan 2018, Han, Kim et al. 2020). However, most of the electrodes were inadequate to use in practical applications due to their poor stability. There are several reports on the enhancement of stability by mixing DSA materials (Han, Kim et al. 2020).

In this study, iron oxide and cobalt oxide were used as an OER suppressor to enhance the CER efficiency in dilute chloride solutions by mixing IrO_2 for enhancing the stability.

1.2. Objectives of the study

To improve the current efficiency for CER in dilute Cl^- solutions, the materials which can suppress OER is proposed as an alternative electrode. Considering the lifetime of the electrodes is the most important factor for practical use, a small amount of DSA was added to enhance the stability.

First, iridium-iron mixed oxide electrode ($0.3IrO_y \cdot 0.7FeO_z$) was fabricated to enhance the current efficiency of CER in dilute chloride solutions. For this purpose, the OER and CER characteristics of the FeO_x, IrO_2, and $0.3IrO_y \cdot 0.7FeO_z$ electrodes were compared. To demonstrate the feasibility of the $0.3IrO_y \cdot 0.7FeO_z$ electrode for practical use, the characteristic of hazardous byproducts formation, stability, and applications to pollutant oxidation in dilute chloride solutions were examined.

Secondly, cobalt oxide was used as another OER suppressor to verify the hypothesis that the materials which have a large difference between the overpotential of OER and CER have the potential to enhance the selectivity of CER. Iridium-cobalt mixed oxide electrode (ICO) was fabricated to enhance the CER efficiency and confirm the validity of the hypothesis.

Chapter 2. Literature Review

2.1. Decrease in efficiency for a chlorine production of dimensionally stable anodes in dilute chloride solutions

Dimensionally stable anodes (DSAs) are the most widely used electrode in electrochemical chlorine production such as chlor-alkali process and water treatment due to their excellent catalytic activity and stability (Kraft, Stadelmann et al. 1999). In Chlor-alkali process, chlorine is electrochemically produced from DSAs in a very high concentration of chloride (almost saturated solutions) for mass production. On the other hand, electrochlorination system for water treatment commonly produces chlorine from naturally derived water such as a river, groundwater, and domestic sewage. The concentration of naturally occurring varies from 10 mg L^{-1} to 250 mg L^{-1} (0.28 mM – 7 mM). Despite the frequent use in dilute chloride solution, most of the studies were conducted using very high chloride concentration. As Kraft et al., pointed out the lack of research on electrochlorination in very dilute chloride solutions, they investigated the dependence of CER efficiency on the concentration of chloride. The iridium oxide (IrO_2–Ta_2O_5) and platinum electrodes with the geometrical areas of 30 cm^{-2} were compared in the circulated electrolyte at 0.3 L min^{-1}. As can be seen in Figure 2-1, the current efficiency for CER was evaluated in the range of chloride concentration from 60

mg L^{-1} to 19000 mg L^{-1} (1.7 mM – 536 mM). Although iridium oxide showed higher efficiency than platinum electrode at all concentrations, the current efficiency of iridium oxide severely decreased below 5000 mg L^{-1} (141 mM). At 60 mg L^{-1} of chloride solution, the current efficiency of IrO_2 was only 4.6%.

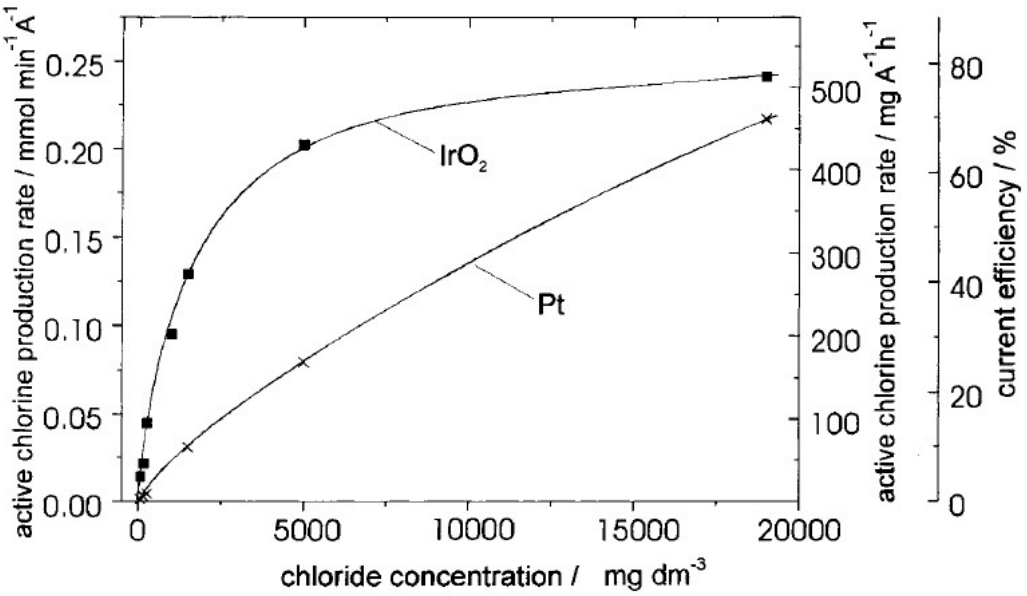

Figure 2-1. Dependence of active chlorine production rate per A with iridium oxide and platinum coated titanium expanded metal electrodes on the chloride concentration (current density 15 mA cm^{-2}, temperature 23 °C) (Kraft, Stadelmann et al. 1999).

2.2. Volcano curve of oxygen evolution reaction

The low efficiency for CER of DSAs is attributed to its low overpotential for OER. Considering OER is the competitive reaction of CER, in dilute chloride solutions, OER becomes more dominant as the electrode produces oxygen more easily. According to "volcano curve" of OER reported by Trasatti (Figure 2-2), the overpotential of OER was plotted as a function of the enthalpy change when the metal oxide is oxidized to a higher oxidation state (Trasatti 1984). The mechanism of OER is known as follows (Hong, Lee et al. 2020):

$$MO_x + H_2O \rightarrow MO_x\,(\cdot OH_{ad}) + H^+ + e^- \quad (2\text{-}1)$$

$$MO_x(\cdot OH_{ad}) \rightarrow MO_{x+1} + H^+ + e^- \quad (2\text{-}2)$$

$$MO_{x+1} \rightarrow MO_x + 1/2\ O_2 \quad (2\text{-}3)$$

Above certain anodic potential, metal oxide (MO_x) would react with water to form adsorbed hydroxyl radical ($\cdot OH_{ad}$) as the first step of OER. After that, $MO_x(\cdot OH_{ad})$ would react to form higher oxide (MO_{x+1}) with a double bond (M=O). As the higher oxide (MO_{x+1}) reverts to the lower oxide, oxygen evolves.

Based on the OER mechanism, metal oxides whose transition enthalpy is much negative such as iron oxide and cobalt oxide are easily oxidized to higher oxides but oxygen atom is too strongly adsorbed to be released as oxygen gas, resulting in

poor OER activity. On the other hand, metal oxides with relatively positive transition enthalpy such as PbO_2, NiO_x, MnO_2, and PtO_2 are unfavorable to form higher oxide because $\cdot OH_{ad}$ is too weakly adsorbed. This also causes poor OER activity. Therefore, the metal oxides with adequate transition enthalpy such as IrO_2 and RuO_2 would show optimal activity for OER. The optimal catalytic activity for OER of DSAs causes a severe decrease in CER efficiency in dilute chloride solution.

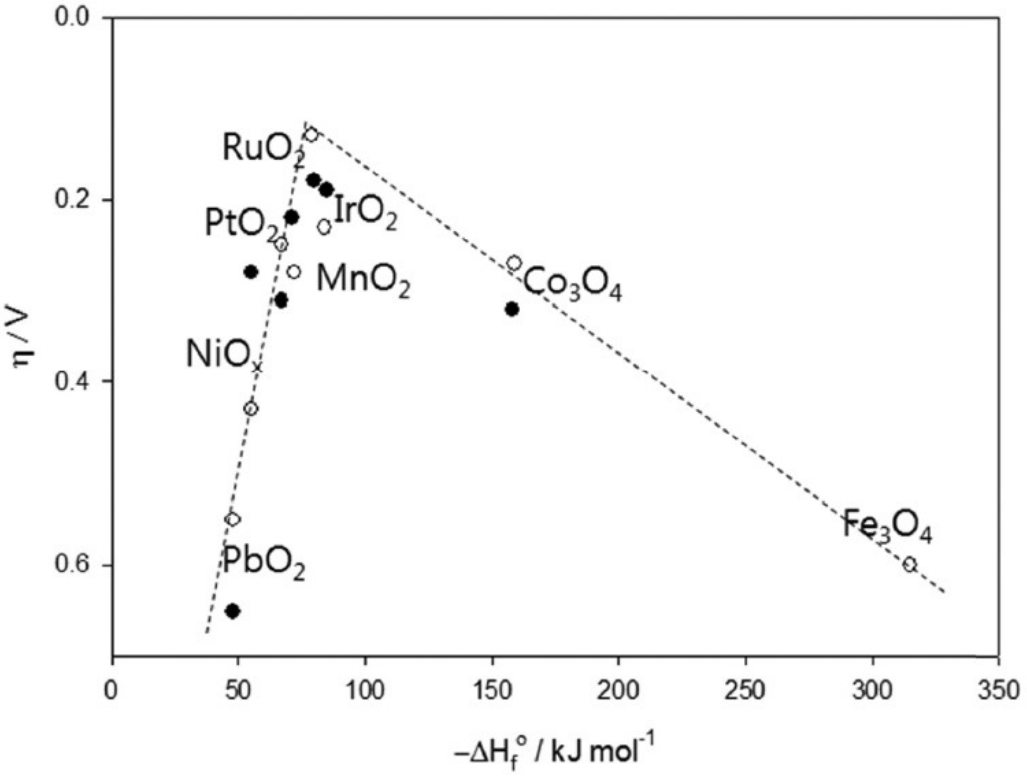

Figure 2-2. Electrocatalytic activity in O_2 evolution at various oxide electrodes as a function of the enthalpy of the lower to higher oxide transition. (○) Alkaline and (●) acid solutions are indicated (Trasatti 1984).

2.3. Iron oxide as a suppressor of oxygen evolution

Iron oxide can be a good candidate for efficient CER in dilute chloride solutions due to its slow reaction rate and large overpotential for OER. Iron oxide is widely used as photoanode material for photoelectrochemical water splitting due to its various advantages such as small band gap (2.0 eV) which can absorb visible light, abundance, and excellent chemical stability in water (Yang, Kang et al. 2014). Despite these advantages, iron oxide has an intrinsic drawback of the slow kinetics of OER with large overpotential (Cong, Chen et al. 2014, Fu, Jiang et al. 2014, Yang, Kang et al. 2014, Tamirat, Su et al. 2015, Zeng, Bai et al. 2015, Carroll and Gamelin 2016). Plenty of research has been conducted to enhance the kinetics of OER by modifying its surface characteristics via various methods. At a different point of view, however, slow kinetics for OER of iron oxide can be a clue to improve CER efficiency in dilute chloride solutions by suppressing the competitive reaction of CER.

From the aforementioned paper of Trasatti (Trasatti 1984), there is another evidence that iron oxide can enhance the CER efficiency in dilute chloride solution. As shown in Figure 2-3, Trasatti also proposed the linear correlation between OER and CER by plotting the working potential for CER against that for OER. In other words, the metal oxide which has a low overpotential of OER would have a low overpotential of CER and vice versa. The author concluded that electrode materials

barely affect selectivity for CER. However, even in that linear correlation, there is a distinctive difference between the working potentials of OER and CER. Iron oxide showed relatively higher OER working potential than CER compared with other metal oxides. It can be a clue to improve the CER efficiency in dilute chloride solutions. The author also added that the situation may differ in low concentration of chloride. Not only iron oxide but also cobalt oxide can be another candidate for improving CER efficiency in dilute chloride solution. Although the overpotential for OER of cobalt oxide is not as high as that of iron oxide, the difference between the OER and CER working potential is comparably large as that of iron oxide. This implies that cobalt oxide can enhance the CER selectivity as effectively suppress OER.

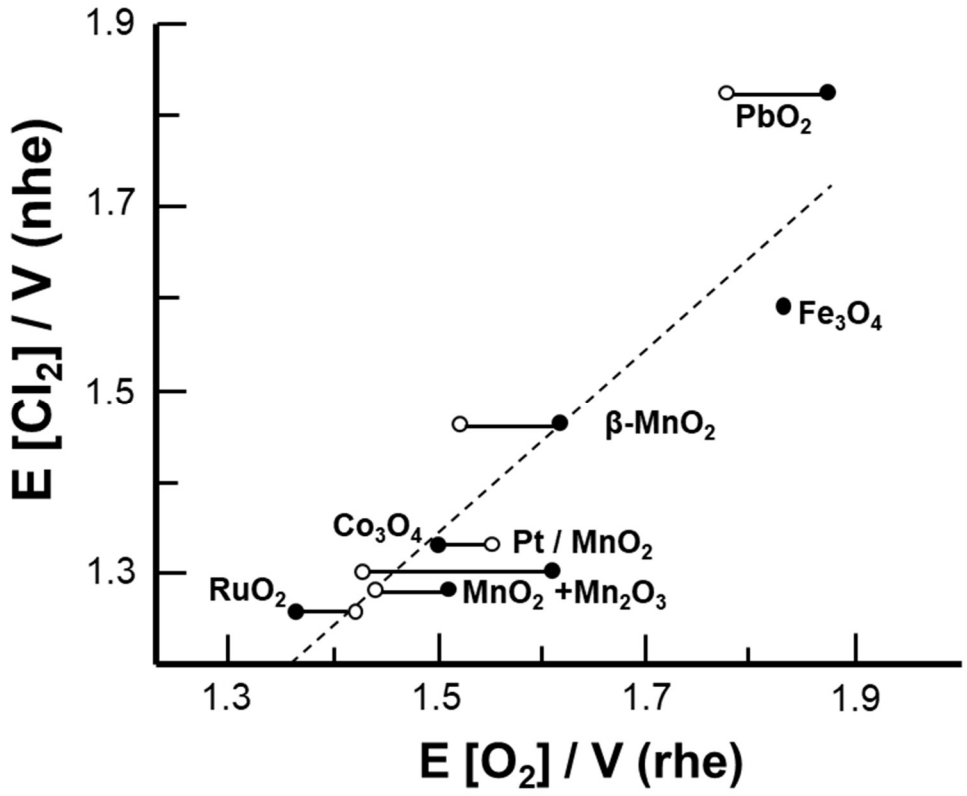

Figure 2-3. Plot of the potential for Cl_2, against the potential for O_2 evolution at the same current density for a number of oxides. (○) Alkaline and (●) acidic solutions are indicated (Trasatti 1984).

2.4. Requisite for the reliable stability of the electrodes

Lifetime is one of the most important requisites of the electrode. Two ways for the loss of the electrocatalytic activity were suggested as follows (Panić, Dekanski et al. 2000, Yi, Kangning et al. 2007):

1. the simultaneous electrochemical oxidation of active material forming the soluble products that move to the electrolyte

2. the formation of insulating TiO_2 layer at the substrate/coating interface which grows by oxidation of the Ti substrate with oxygen

Based on the deterioration mechanism, adsorption/desorption of oxygen atom should be fast and reversible for a long lifetime (refer to Equation (2-1) − (2-3)), otherwise side reactions such as oxidation of active material and substrate would occur. This is the reason that DSAs show reliable stability. Between IrO_2 and RuO_2, IrO_2 is known to be more stable because the soluble product of IrO_2 (IrO_3) is less favorably formed than that of RuO_2 (RuO_4) (Moser, Mondelli et al. 2013).

2.5. Volcano curve of chlorine evolution reaction

To elucidate the electrocatalytic activity for CER, Zeradjanin et al. proposed the volcano curve of CER by utilizing the vibrational frequency of the crystal lattice as a dynamic descriptor instead of the thermodynamic descriptor as transition enthalpy (Figure 2-4) (Zeradjanin, Menzel et al. 2012). They insisted that the formation of an OH_{ad} layer resulting from water is a prerequisite for CER based on the sluggish CER in non-aqueous solutions. The pathways for CER is known as follows:

$$MO_x + H_2O \rightarrow MO_x\,(\cdot OH_{ad}) + H^+ + e^- \quad (2\text{-}4)$$

$$MO_x(\cdot OH_{ad}) + Cl^- \rightarrow MO_x\,(\cdot OHCl_{ad}) + e^- \quad (2\text{-}5)$$

$$MO_x(\cdot OHCl_{ad}) + Cl^- + H^+ \rightarrow MO_x + Cl_2 + H_2O \quad (2\text{-}6)$$

Based on the pathways for CER, the authors suggested the importance of the nature and strength of the interaction between a metal oxide and adsorbed oxygen from the water molecule ($\cdot OH_{ad}$). In addition, Rossmeisl et al. also suggested that the binding energy between the metal atom in metal oxide and adsorbed oxygen atom is a universal catalytic descriptor for the CER and OER (Hansen, Man et al. 2010). Zeradjanin et al. suggested that the vibrational frequency in the Cl−O bond should be very similar to that of M−O for optimal CER, considering the timescales of electron transfer and vibrations are similar, a vibrational energy change would

easily happen if the two vibrational wave functions are more overlapped. The authors compared the vibrational frequency of metal oxides with that of Cl−O using Raman spectroscopy and plotted the volcano curve of CER. As shown in Figure 2-4, the metal oxides whose Raman shift is similar to Cl−O such as IrO_2 and RuO_2 would exhibit excellent CER activity.

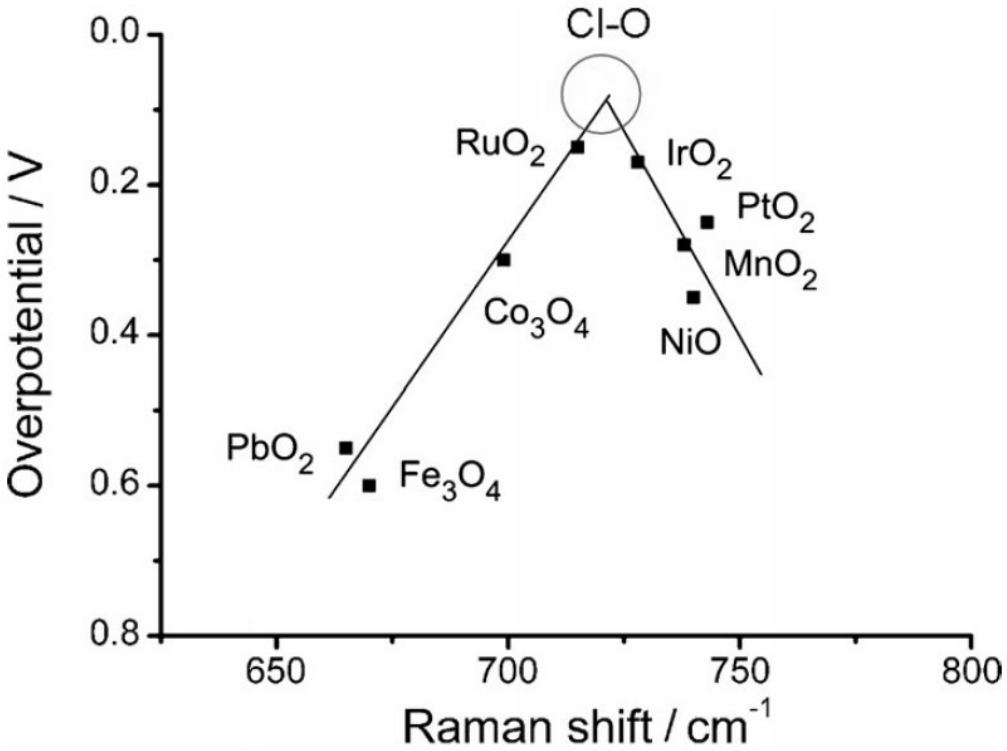

Figure 2-4. Overpotentials of the CER as a function of the characteristic Raman shifts. The top of the volcano curve marked with the circle corresponds to the Raman shift of the Cl−O bond vibration of HClO in aqueous solution (Zeradjanin, Menzel et al. 2012).

2.6. Necessity of arsenite oxidation process

Arsenic contamination in groundwater has been a serious problem in many countries including India, Bangladesh, Argentina, USA, Taiwan, and Japan, etc (Lakshmipathiraj, Prabhakar et al. 2010). Since the prolonged intake of arsenic from drinking water causes lung cancer, neurological disorder, and hyperkeratosis, the World Health Organization (WHO) recommends that the maximum concentration of arsenic in drinking water should be lower than 10 μL^{-1} (Sorlini and Gialdini 2010, Lacasa, Cañizares et al. 2012). However, several hundred billions people still drink contaminated water with arsenic above the WHO standard.

Arsenic in groundwater generally occurs from the dissolution of arsenic minerals. The main forms of arsenic are inorganic arsenite (As(III)) and arsenate (As(V)). In groundwater, arsenite is predominantly present due to its anaerobic condition. Arsenite is known to be 60-times more toxic than arsenate (Du, Zhang et al. 2013). In addition, arsenite is much more difficult to remove with conventional treatment such as coagulation–filtration, adsorption, and ion exchange because arsenite exists as the non-ionic H_3AsO_3 up to pH 9.2. On the other hand, arsenate exists as the arsenate anions ($H_2AsO_4^-$, $HAsO_4^{2-}$, and AsO_4^{3-}) above pH 2.2. Therefore, arsenite oxidation to arsenate is a prerequisite for effective arsenic removal. Strong oxidants are generally used to oxidize arsenite because the oxidation rate of arsenite is extremely sluggish. Among various oxidants, chlorine is reported as an effective

reagent (Sorlini and Gialdini 2010). Alum precipitation is known as the most effective arsenic removal process if an oxidant is added ahead below pH 7 (Kartinen Jr and Martin 1995). Figure 2-5 shows the effect of chlorine dose on the removal efficiency of arsenic using alum. After the oxidation process with chlorine below pH 7, about 90% of arsenic was removed by alum precipitation. On the other hand, only 10% of the arsenic was removed without chlorine. Only 10% of the arsenic was removed without chlorine

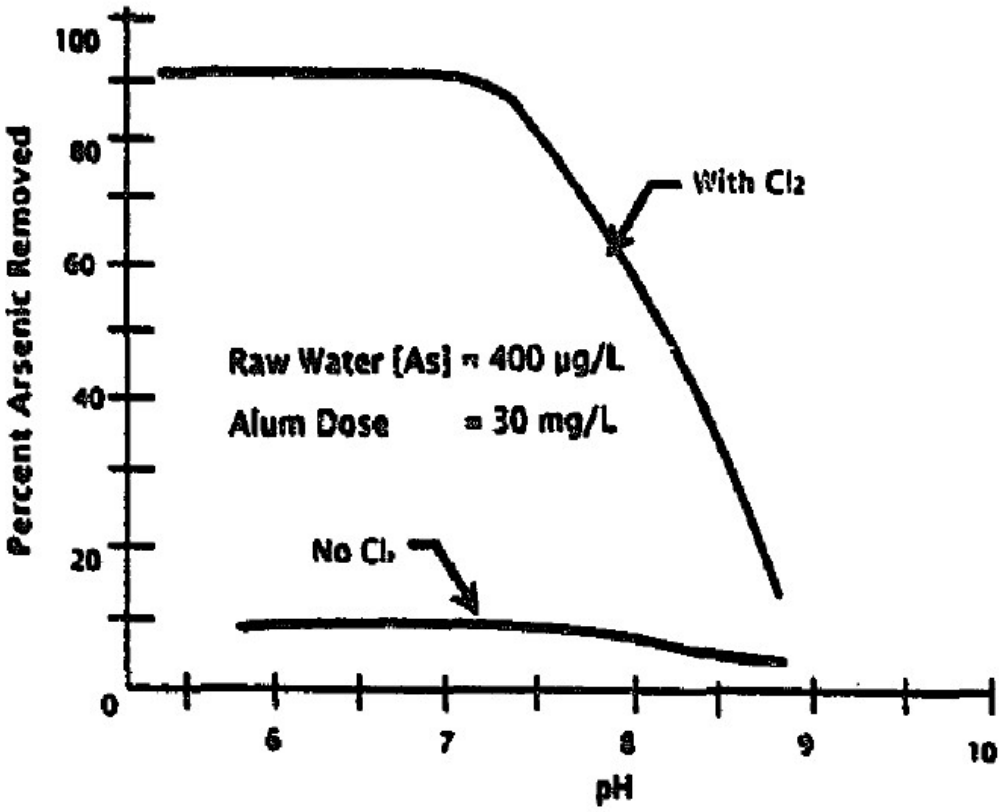

Figure 2-5. Effect of chlorine dose on the removal efficiency of arsenic using alum (Kartinen Jr and Martin 1995).

Chapter 3. Iridium-iron mixed oxide electrode as a highly efficient electrode for electrochlorination in dilute chloride solutions

3.1. Introduction

To improve the CER efficiency of DSA in dilute chloride solution, iron oxide was adopted as a co-catalyst to suppress OER because it has an extremely slow reaction rate of OER with a high OER overpotential (Sivula, Le Formal et al. 2011, Spray, McDonald et al. 2011, Rahman and Joo 2012, Cong, Chen et al. 2014, Fu, Jiang et al. 2014, Yang, Kang et al. 2014, Tamirat, Su et al. 2015, Zeng, Bai et al. 2015, Carroll and Gamelin 2016). In addition, according to the previous study (Trasatti 1984), iron oxide had a much higher working potential for OER than that for CER, which can be interpreted as iron oxide has high selectivity for CER against OER. Furthermore, iron oxide showed a relatively larger difference in the working potential between the OER and CER compared with other metal oxides. These characteristics of iron oxide can be an indication that iron oxide has more potential to improve the CER efficiency in dilute Cl^- solutions than other metal oxides. Nevertheless, to the best of our knowledge, iron oxide has not been investigated as an OER suppressor for efficient CER on DSA, especially in dilute Cl^- solutions.

Therefore, in this study, we aimed to improve the CER efficiency of IrO_2 as a representative of DSA in dilute Cl^- solutions by addition of iron oxide (FeO_x) as a co-catalyst and to elucidate the electrocatalytic behavior of the iridium-iron mixed oxide electrode ($0.3IrO_y{\cdot}0.7FeO_z$). The formation characteristic of hazardous inorganic byproducts and lifetime of the $0.3IrO_y{\cdot}0.7FeO_z$ electrode were also investigated to confirm the viability for practical use. In addition, the feasibility of environmental application for electrochlorination was also demonstrated through the arsenite oxidation process, ammonium removal, and direct electrolysis of tap water.

3.2. Materials and methods

All chemicals were of reagent grade and were purchased from Sigma-Aldrich Co. and used without further purification. Deionized (DI) water (18.2 MΩ·cm, Milli-Q® Direct 8 system, Merck Millipore, MA, USA) was used to prepare the solutions.

3.2.1. Preparation of the electrodes

The electrodes for CER were fabricated with a working area of 1 cm × 1.5 cm by thermal decomposition. To fabricate the FeO_x, IrO_2, and RuO_2 electrodes, the precursor solutions of the electrodes were prepared as follows: 1.6 g $FeCl_3$, 0.8 g $IrCl_3 \cdot xH_2O$, and 0.5 g $RuCl_3 \cdot xH_2O$ were respectively dissolved in a solvent comprising 5 mL DI water and 5 mL ethanol. In addition, the iridium-iron mixed oxide electrodes were fabricated with various volume percentages (v/v%) of the precursor solutions of FeO_x and IrO_2 (1%, 3%, 5%, 10%, 40%, 70%). Titanium foil (Ti) as a substrate was sandpapered and etched in 37% HCl at 60 °C for 30 min. The substrate was rinsed with DI water and dried. The precursor solution (33 μL) was poured onto the Ti substrate and spin-coated using a spin-coater (Model WS-400BZ-6NPP/Lite, Laurell Technologies Co., PA, USA) for 15 s at 100 rpm. The electrodes were dried at 100 °C to evaporate the solvent for 5 min and annealed at 500 °C for 5 min. The spin-coating and annealing processes were repeated four times. Finally, the electrodes were annealed at 500 °C for 4 h under atmospheric conditions.

To compare the iridium-iron mixed oxide electrodes and a simple mixture of FeO_x and IrO_2, the simple mixture electrode of FeO_x and IrO_2 (FeO_x+IrO_2) was fabricated as follows. The bottom part (1.0 cm × 0.4 cm) of the as-prepared FeO_x was scraped and etched in 37% HCl at 60 °C for 20 min. After rinsing with DI water and drying,

the precursor solution of IrO_2 was spin-coated. The electrode was dried at 100 °C for 5 min and annealed at 500 °C for 5 min. The spin-coating and annealing processes were repeated four times. Finally, the electrode was annealed at 500 °C for 4 h.

3.2.2. Characterization of the electrodes

The microstructures and chemical compositions of the as-prepared electrodes were investigated by field emission scanning electron microscope (FE-SEM) coupled with an energy-dispersive X-ray spectroscopy (EDS) system (JSM-7800F Prime, JEOL Ltd, Japan). The crystal structure of the electrodes was determined using an X-ray diffractometer (SmartLab, Rigaku, Tokyo, Japan) with Cu Kα radiation (40 kV, 250 mA) in the 2θ range of 10° – 80° at a scan rate of 2° s^{-1}. The surface characteristics of the electrodes were analyzed using X-ray photoelectron spectroscopy (XPS) performed in an UHV multipurpose surface analysis system (Sigma probe, Thermo, UK) operated at a base pressure of less than 10^{-9} mbar. The photoelectron spectra were excited by an Al Kα (1486.6 eV) anode operating at a constant power of 150 W (15 kV and 10 mA). Raman spectroscopy measurements were conducted to plot the so-called "volcano curve" of CER with a Raman spectrometer (DXR2xi, laser wavelength of 532 nm). To measure the vibration of the Cl−O bond, the hypochlorous acid sample was prepared electrochemically with IrO_2 in 10 mM NaCl at a current density of 10 mA cm^{-2} for 20 min.

3.2.3. Electrochemical measurements

Electrochemical impedance spectroscopy (EIS) was conducted using a potentiostat (VersaSTAT 3, Princeton Applied Research, USA). The rest of electrochemical experiments were performed using a battery cycler (WBC3000, WonATech, Seoul, Korea). Linear sweep voltammetry (LSV), EIS, and electrode potential measurements were conducted using a three-electrode system. A Pt electrode was used as a counter electrode, and an Ag/AgCl (KCl sat.) electrode was used as the reference electrode. The rest of the experiments were conducted with a two-electrode system with a Pt electrode unless otherwise stated.

3.2.3.1. Electrochemical chlorine evolution

The experiments for CER on iridium-iron mixed oxide electrodes, IrO_2, and FeO_x electrodes were performed at a current density of 10 mA cm^{-2} for 5 min in a 30 mL aqueous solution at a stirring rate of 200 rpm. The concentration of Cl_2 was measured as total chlorine using the N,N-diethyl-p-phenylenediamine (DPD) method with a colorimeter (DR 900, HACH Co., USA). The current efficiency for CER was calculated as follows:

$$\text{Current efficiency for CER (\%)} = (C \cdot V \cdot n \cdot F) / (j \cdot A \cdot t) \times 100 \quad (3\text{-}1)$$

, where C is the concentration of Cl_2 (mol L^{-1}), V is the volume of the solution (L), n is the number of electrons participating in CER (2 equiv. mol^{-1}), F is the Faraday constant (96485 C equiv.$^{-1}$), j is the current density (A cm^{-2}), A is the area of the electrode (cm^2), and t is the electrolysis time (s).

3.2.3.2. Linear sweep voltammetry

To investigate the electrocatalytic activity for CER and OER, LSV was performed at a scan rate of 2 mV s^{-1} in the potential range of 0.8 V to 1.6 V (vs. Ag/AgCl). The onset potential in LSV was defined as the potential at a current density of 0.5 mA cm^{-2}. To explicate the behavior of the as-prepared electrodes for CER and OER in a concentrated solution, 2 M NaCl and 2 M $NaNO_3$ aqueous solutions were used, respectively. On the other hand, in a dilute Cl^- solution, it is difficult to distinguish CER from OER due to the co-occurrence of both reactions. Therefore, 10 mM HCl and 10 mM HNO_3 solutions were used to distinguish between the two reactions because the OER can be more suppressed at lower pH value (Sohrabnejad-Eskan, Goryachev et al. 2017, Vos, Liu et al. 2019).

3.2.3.3. Long-term stability test

The stability test was performed in the tap water of Seoul, Korea, at a current density of 20 mA cm^{-2}. The tap water was supplied directly and continuously to the system. The Cl_2 production rate was calculated as follows:

Cl_2 production rate (mg h^{-1}) = Cl_2 concentration (mg L^{-1}) × flow rate (L h^{-1}) (3-2)

3.2.3.4. Accelerated stability test

To examine the stability of iridium-iron mixed oxide electrodes, an accelerated stability test was conducted in 30 mL of 0.5 M H_2SO_4 solution at 0.5 A cm^{-2} for 200 hours with Pt counter electrode

3.2.3.5. Cyclic voltammetry

To measure the electrochemically active surface area, cyclic voltammetry (CV) was conducted in 50 mM NaCl in the potential range of 0.2 – 1.0 V at a scan rate of 20 mV s^{-1}.

3.2.3.6. Electrochemical impedance spectroscopy

EIS was conducted in 2 M NaCl and 2 M $NaNO_3$ at 1.4 V (vs. Ag/AgCl) with 10 mV amplitude covering the frequency region of 50 Hz – 50000 Hz to measure charge transfer resistance (R_{ct}) for CER and OER.

3.2.3.7. Byproducts formation

To evaluate the safety of the iridium-iron mixed oxide electrodes, the characteristics of byproducts formation were investigated. Electrochlorination was conducted in 30 mL of 4 mM NaCl at various current densities of 5, 10, 20, and 30 mA cm^{-2}. The produced byproducts (chlorite, chlorate, perchlorate) were measured

with ion chromatography (DX-120, Thermo Fisher Scientific Inc).

3.2.3.8. Arsenite oxidation

To demonstrate the feasibility of the application of electrochlorination system to arsenite oxidation, the experiment was conducted with an initial concentration of 300 μM of $NaAs(III)O_2$ with varying the supporting electrolyte at a current density of 10 mA cm^{-2}. To investigate the effect of chlorine on arsenite oxidation, the electrolysis was conducted in 1 mM NaCl or 1 mM $NaNO_3$. In addition, arsenite oxidation was conducted in 1 mM, 10 mM, and 20 mM NaCl to investigate the effect of chloride concentration on arsenite oxidation rate. The concentration of arsenic was measured using a molybdenum blue method with a UV/Vis spectrometry at a wavelength of 865 nm (Agilent 8453, Agilent, USA) (Tsang, Phu et al. 2007).

3.2.3.9. Ammonium removal

Ammonium removal in a dilute chloride solution was performed in 30 mL of 1 mM NH_4Cl aqueous solution at a current density of 10 mA cm^{-2} to examine the feasibility of $0.3IrO_y{\cdot}0.7FeO_z$ for water treatment in domestic sewage. Ammonium ions were measured by ion chromatography (ICS-1100, Thermo Fisher Scientific Inc).

3.3. Results and Discussion

3.3.1. Characterization of the FeO_x electrode

To confirm the formation of the iron oxide, iridium oxide, and ruthenium oxide on Ti substrate, the crystal structure of the electrodes was analyzed with XRD (Figure 3-1). From the XRD data of the as-prepared iron oxide electrode in Figure 3-1a, it appears that iron oxide was comprised of Fe_2O_3 (hematite), Fe_3O_4 (magnetite), and $Fe_{0.95}O$ (wüstite) (JCPDS PDF# 79-1741, 65-3107, 79-1967). Figure 3-1b and c show that iridium oxide and ruthenium oxide were well fabricated in the form of IrO_2 and RuO_2, respectively (JCPDS PDF# 71-4827 and 75-4303).

Figure 3-2 shows the surface characteristics of the FeO_x electrode examined using SEM and EDS. As shown in Figure 3-2a, FeO_x nanoparticles clustered on the Ti substrate. From the EDS mapping data (Figure 3-2b and c), it can be seen that FeO_x nanoparticles are evenly distributed on the Ti substrate. Figure 3-2d shows that the composition of FeO_x was $Fe_{0.47}O_{0.53}$.

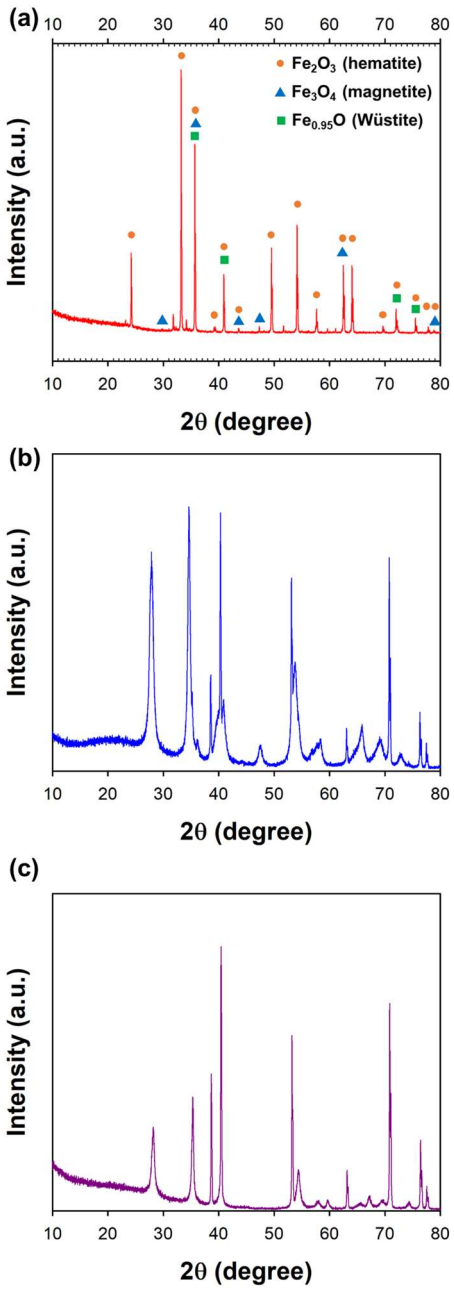

Figure 3-1. X-ray diffraction patterns of the as-prepared FeO_x, IrO_2, and RuO_2 electrode (JCPDS PDF# 79-1741, 65-3107, 79-1967, 71-4827, and 75-4303, respectively).

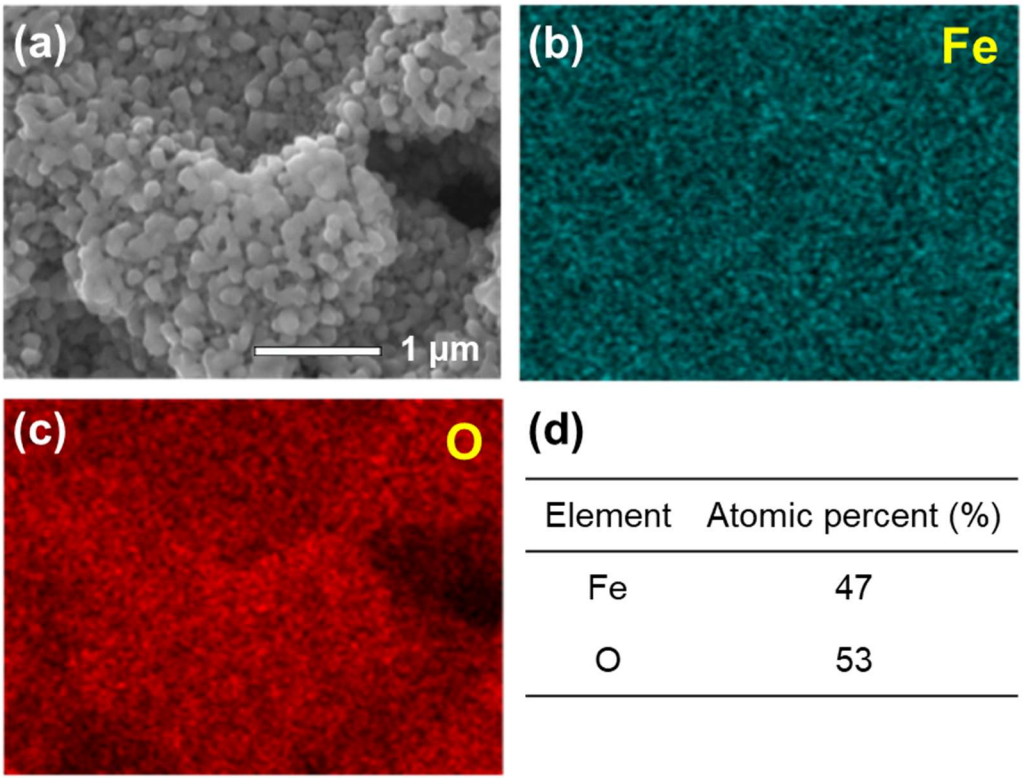

Element	Atomic percent (%)
Fe	47
O	53

Figure 3-2. (a) SEM image, (b) EDS mapping data of the as-prepared FeO_x electrode regarding (b) Fe and (c) O, and quantitative analysis.

3.3.2. Chlorine evolution efficiency of the FeO_x electrode

Figure 3-3 illustrates the current efficiency for CER of the FeO_x, IrO_2, and RuO_2 electrodes at various concentrations of NaCl aqueous solution (1 mM − 2000 mM). The FeO_x electrode showed an outstanding performance of the CER at all ranges of chloride concentrations comparable to that of IrO_2, which is well-known as a superior electrode for CER. On the other hand, RuO_2 known as one of the representative electrodes of DSAs revealed inferior current efficiency for CER at all concentrations. The current efficiency for CER of DSAs (IrO_2 and RuO_2) drastically decreases below the chloride concentration of 200 mM. At the level of fresh water (below 7 mM of chloride concentration), DSAs barely produce chlorine. Interestingly, the current efficiency for the CER of FeO_x is much higher than that of IrO_2 and RuO_2 in the dilute chloride solution (1 mM to 20 mM NaCl). In particular, at a chloride concentration of 1 mM, the current efficiency for CER of FeO_x (16.8%) is 5 times higher than that of IrO_2 (3.2%), and 20 times higher than that of RuO_2 (0.8%).

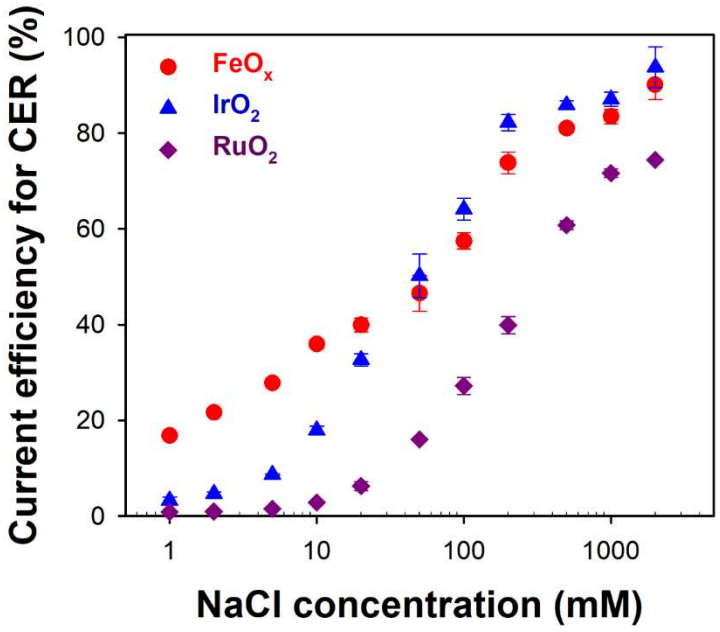

Figure 3-3. Current efficiency for CER of the FeO_x, IrO_2, and RuO_2 electrodes at various concentrations of NaCl aqueous solution (current density: 10 mA cm^{-2}).

3.3.3. Characteristics of CER and OER of the FeO_x electrode

To elucidate the efficient electrocatalytic property of FeO_x for the CER in a dilute chloride solution, LSVs on FeO_x and IrO_2 were measured (Figure 3-4). Note that the red and blue colors represent FeO_x and IrO_2, respectively, and the filled and empty symbols represent the electrolyte in the presence and absence of chloride, respectively. In the concentrated solution (Figure 3-4a), the current density in the 2 M $NaNO_3$ solution originates from the OER, whereas the current density in 2 M NaCl can be assumed to originate from the CER considering that the current efficiencies for CER of FeO_x and IrO_2 are over 90% in 2 M NaCl. As shown in Figure 3-4a, FeO_x exhibits higher overpotentials for CER and OER compared with IrO_2, which is confirmed by the onset potentials for each reaction. In particular, the onset potential for OER is far higher on FeO_x (1.4 V) than IrO_2 (1.1 V), indicating that FeO_x exhibits much slower reaction kinetics for OER than IrO_2. Furthermore, it should be noted that the difference in onset potential between CER and OER is significantly high for FeO_x (172 mV). Considering OER is the competitive reaction to CER, the large potential difference implies that FeO_x has good selectivity for CER over OER. On the other hand, IrO_2 begins to generate Cl_2 and O_2 with a very low onset potential of 1.1 V, implying that IrO_2 has fast kinetics, not only for the CER but also for the OER. Meanwhile, IrO_2 leads to a much higher current increase in CER than in OER, implying that IrO_2 shows a high current efficiency for CER

in chloride-rich environments owing to its extremely fast reaction rate for CER compared with that for OER. In the dilute chloride solution (Figure 3-4b), FeO_x exhibits a large difference of 70 mV in the onset potential between CER and OER, whereas IrO_2 exhibits no difference. This indicates that FeO_x shows a relatively higher selectivity for CER, while IrO_2 mostly produces OER in dilute chloride solutions. The electrocatalytic behavior of RuO_2 is very similar to that of IrO_2 (Figure 3-5). The results suggest that in a chloride-deficient environment, the current efficiency for CER is greatly affected by slow OER kinetics and the large difference in onset potential between CER and OER, as compared with fast CER kinetics.

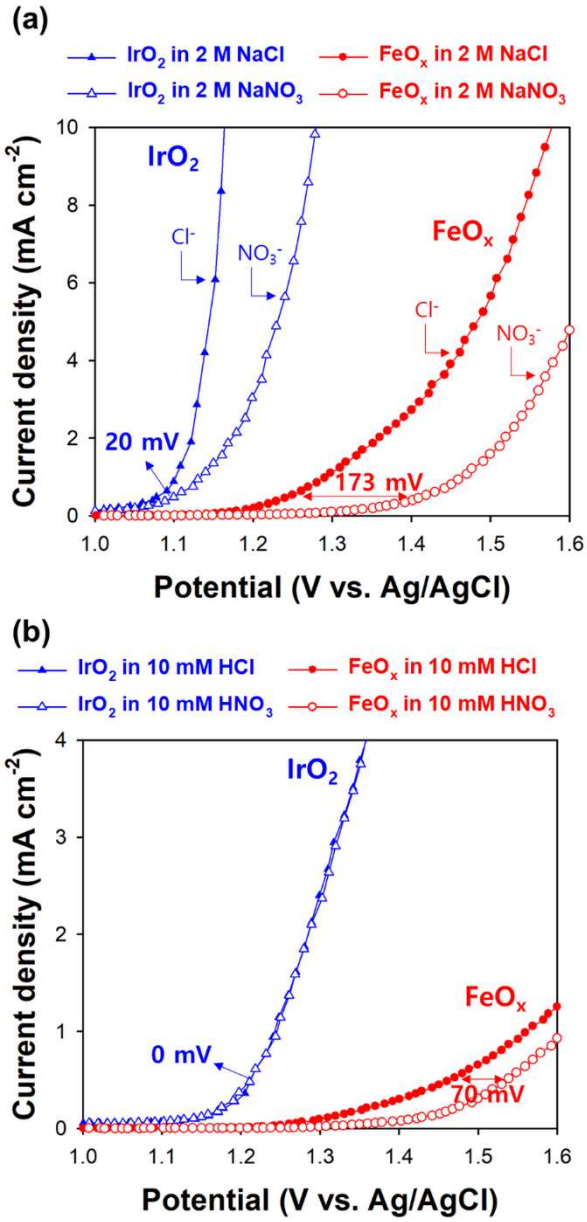

Figure 3-4. Linear sweep voltammograms of FeO_x and IrO_2 (a) in highly concentrated aqueous solutions (NaCl (2 M) and $NaNO_3$ (2 M)) and (b) in dilute solutions (HCl (10 mM) and HNO_3 (10 mM)), respectively (scan rate: 2 mV s^{-1}).

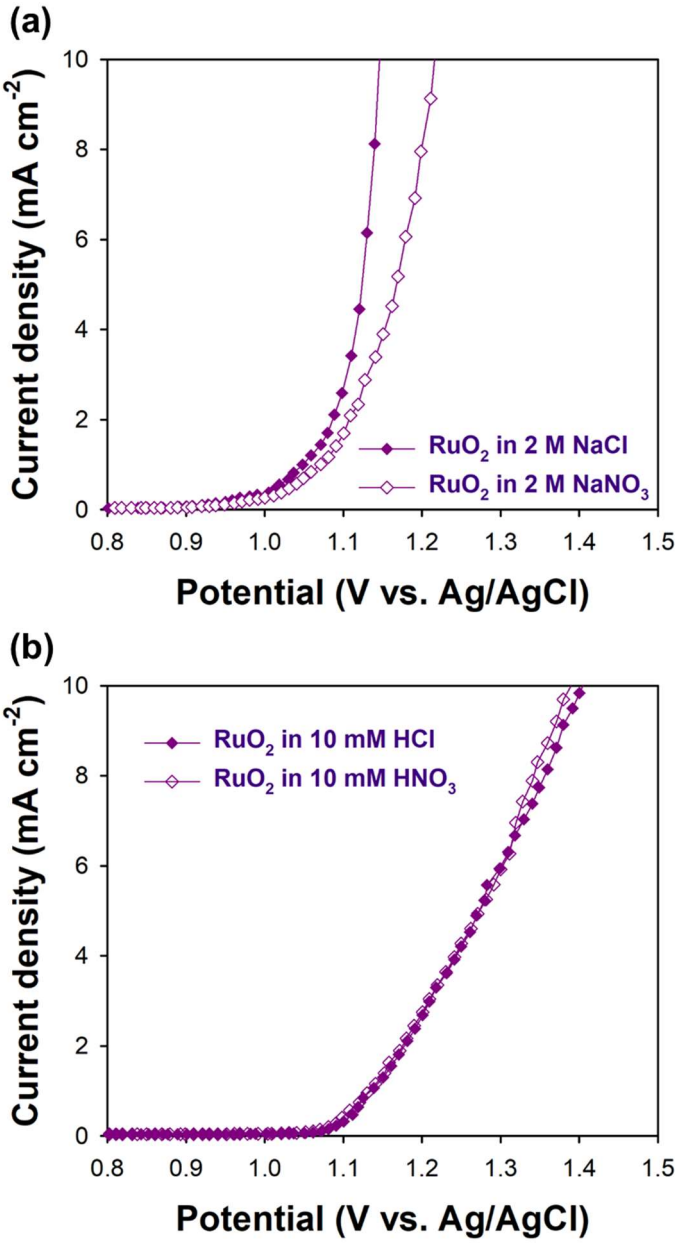

Figure 3-5. Linear sweep voltammograms of the RuO_2 electrodes (a) in the highly concentrated aqueous solutions (NaCl (2 M) and $NaNO_3$ (2 M)) and (b) in the dilute solutions (HCl (10 mM) and HNO_3 (10 mM)), respectively (scan rate: 2mV s^{-1}).

3.3.4. Stability of the FeO_x electrode

Figure 3-6 shows the voltage profiles of the FeO_x-Pt and IrO_2-Pt systems during the tap water electrolysis to examine the long-term stability of FeO_x compared with IrO_2. The composition of the tap water is listed in Table 3-1. The voltage profile of the FeO_x-Pt system drastically increased within 20 h indicating the loss of the electrocatalytic activity of the FeO_x electrode. On the other hand, the voltage profile of the IrO_2-Pt system was stably retained over 28 days. This result shows that the lifetime of the FeO_x electrode is too short and inadequate for practical use. It can be concluded that the long-term stability of the FeO_x electrode should be improved for the successful practical use of electrochlorination.

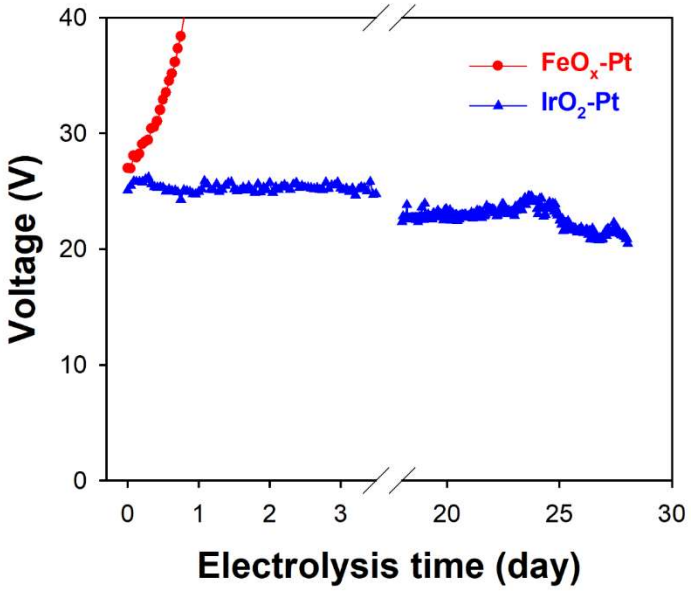

Figure 3-6. Voltage profiles of the FeO_x–Pt and IrO_2–Pt systems during the electrolysis of tap water in Seoul, Korea (current density: 20 mA cm^{-2}).

Table 3-1. Composition of tap water in Seoul, Korea.

$[Cl^-]$ (mM)	0.75
$[SO_4^{2-}]$ (mM)	0.15
$[NO_3^-]$ (mM)	0.15
$[Na^+]$ (mM)	0.52
$[K^+]$ (mM)	0.06
$[Mg^{2+}]$ (mM)	0.33
$[Ca^{2+}]$ (mM)	0.62
pH	7.5
Residual Cl_2, C_i, (mg L^{-1})	0.03
Conductivity (mS cm^{-1})	0.217

3.3.5. Fabrication of the iridium-iron mixed oxide electrodes

Our strategy for improving the long-term stability of the FeO_x electrode is the introduction of IrO_2 as a co-catalyst, which is very stable and well-known as a mediator for electron shuttling in mixed oxide electrodes. The iridium-iron mixed oxide electrodes were fabricated with various composition ratios. Figure 3-7a shows the current efficiency for CER of the iridium-iron mixed oxide electrodes. Interestingly, the iridium-iron mixed oxide electrodes showed far improved CER efficiency than pristine IrO_2 and FeO_x electrodes. Among them, the electrode with 70 at.% of Fe (Fe:Ir = 70:30) showed the most efficient CER performance. Figure 3-7b illustrates the voltage profiles of the iridium-iron mixed oxide electrodes with Pt counter electrode during the accelerated stability test in 0.5 M H_2SO_4 at 0.5 A cm^{-2}. Except for the electrode with the smallest Ir component (92 at.% of Fe), all electrodes stably retained their voltage profiles. After the accelerated stability test, the current efficiency for CER was measured under the same experimental conditions. Although there was overall deterioration in CER performance, the electrode with 70 at.% of Fe maintained the highest CER efficiency. As a representative of the iridium-iron mixed oxide electrodes, the electrode with 70 at.% of Fe was chosen to investigate CER performance and electrocatalytic behavior resulting from the addition of FeO_x into IrO_2.

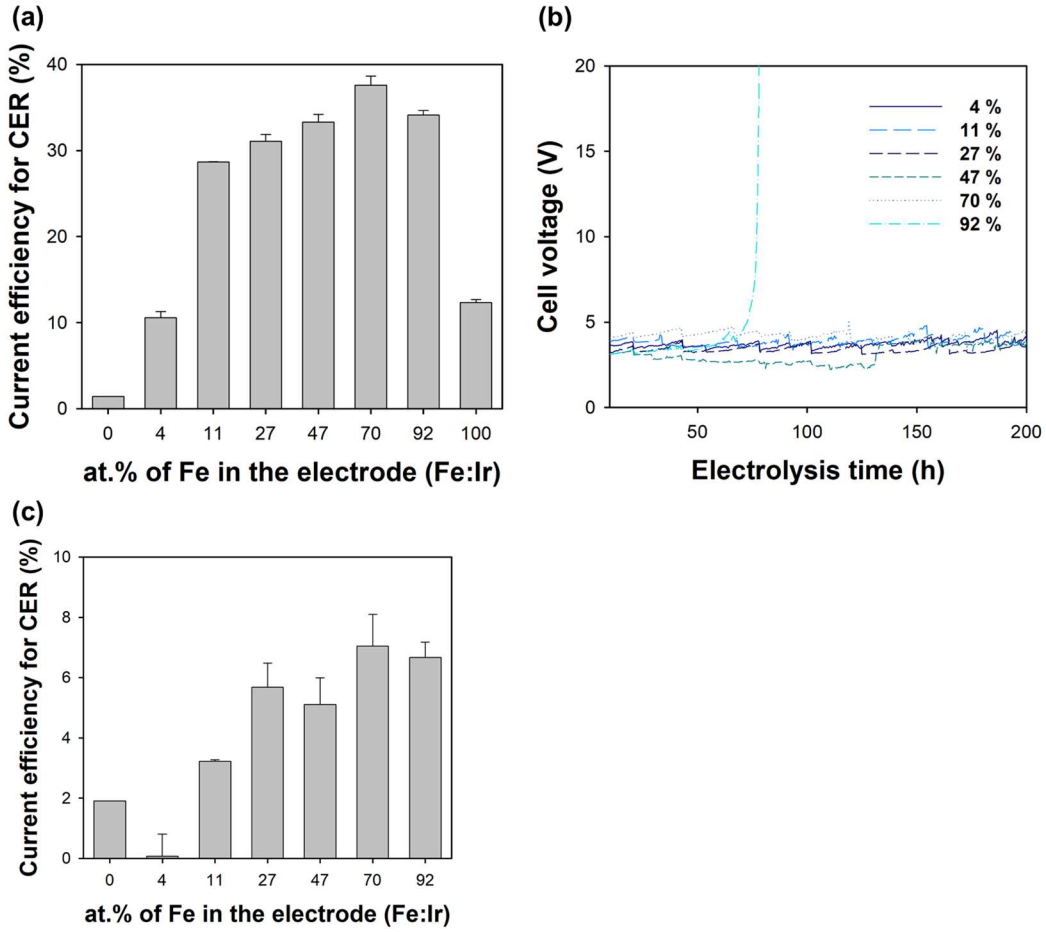

Figure 3-7. (a) Current efficiency for the CER of the iridium-iron mixed oxide electrodes with various atomic ratios (Fe:Ir) (1 mM NaCl, current density of 10 mA cm^{-2}). (b) Voltage profile during the accelerated stability test of the iridium-iron mixed oxide electrodes with Pt counter electrode (0.5 M H_2SO_4, 0.5 A cm cm^{-2}.). (c) Current efficiency for the CER of the iridium-iron mixed oxide electrodes after the accelerated stability test (1 mM NaCl, current density of 10 mA cm^{-2}).

3.3.6. Characterization of the $0.3IrO_y \cdot 0.7FeO_z$ electrode

From the quantitative analysis with EDS (Figure 3-8a), the iridium-iron mixed oxide electrode with 70 at.% of Fe will be denoted as $0.3IrO_y \cdot 0.7FeO_z$. Figure 3-8 b, c, and d confirm that Ir and Fe components were evenly distributed in the $0.3IrO_y \cdot 0.7FeO_z$ electrode. Figure 3-9a represents the XRD patterns of the $0.3IrO_y \cdot 0.7FeO_z$ electrode, mainly showing the characteristic peaks of IrO_2, Fe_2O_3, and Ti. Figure 3-9b, c, and d show the SEM images of $0.3IrO_y \cdot 0.7FeO_z$, IrO_2, and FeO_x, respectively. $0.3IrO_y \cdot 0.7FeO_z$ shows uniform nano-grains onto the electrode surface. Considering the IrO_2 and FeO_x electrode surfaces, it seems that the IrO_2 nanoparticles are evenly distributed on the FeO_x particles. This leads to an improvement in electrochemically active surface area of $0.3IrO_y \cdot 0.7FeO_z$ compared with that of IrO_2 and FeO_x (Figure 3-10). Integrated charge in CV has been regarded as an indicator of electrochemically active surface area. $0.3IrO_y \cdot 0.7FeO_z$ showed the highest current response during CV, followed by IrO_2, and FeO_x. From the CVs, integrated charge of $0.3IrO_y \cdot 0.7FeO_z$, IrO_2, and FeO_x was 8.8 mC cm^{-2}, 5.5 mC cm^{-2}, and 0.1 mC cm^{-2}, respectively (Figure 3-10b). These results imply that $0.3IrO_y \cdot 0.7FeO_z$ has the largest electrochemically active surface area.

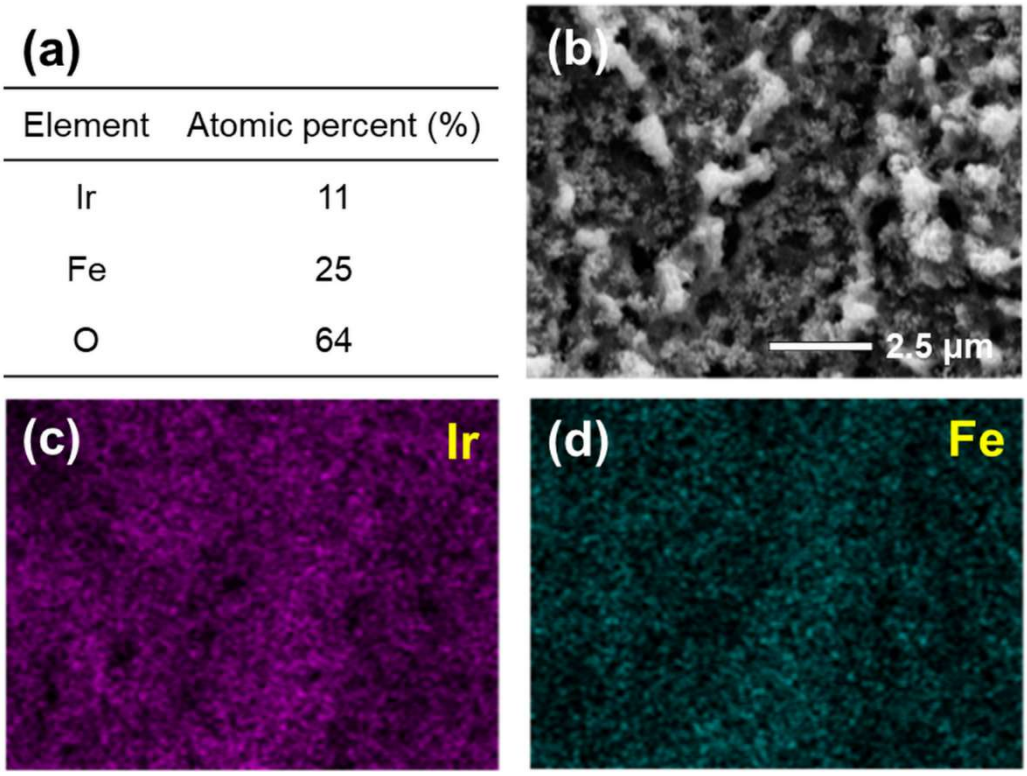

Figure 3-8. EDS data of the iridium-iron mixed oxide electrode with 70 at.% of Fe: (a) quantitative analysis, (b) SEM image, and EDS maps of (c) Ir and (d) Fe.

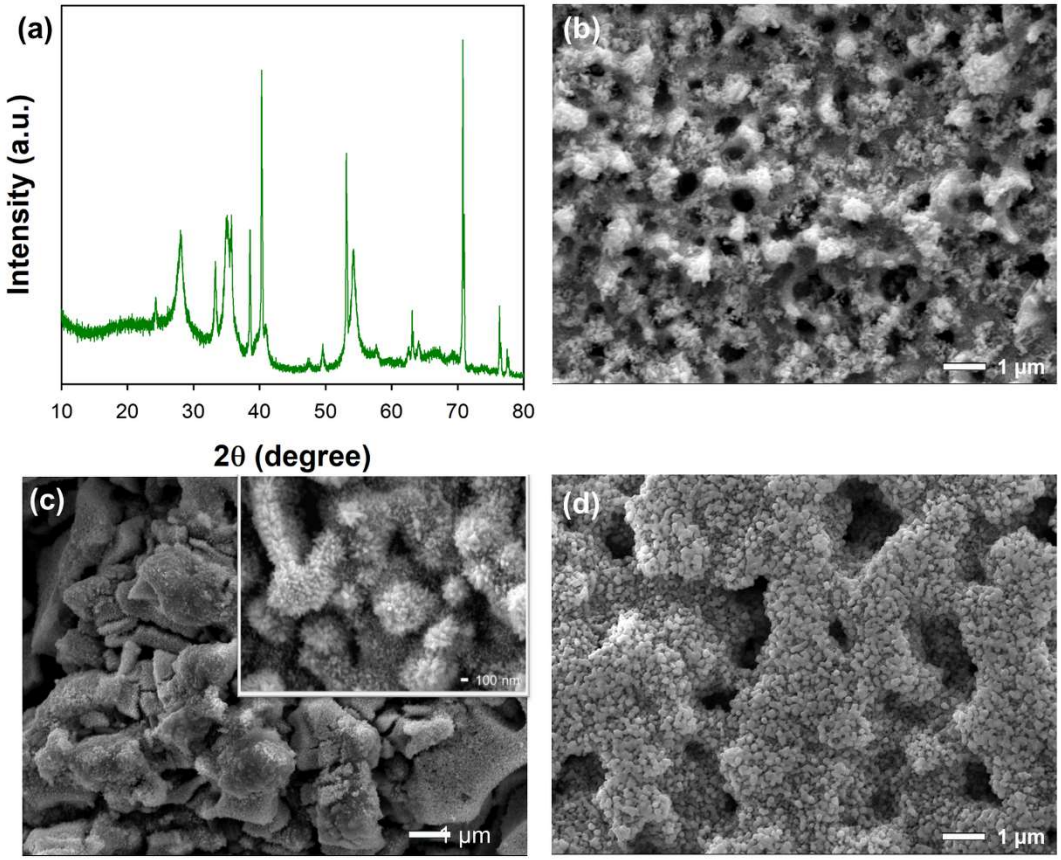

Figure 3-9. (a) XRD patterns of the as-prepared $0.3IrO_y \cdot 0.7FeO_z$ electrode. SEM images of (b) $0.3IrO_y \cdot 0.7FeO_z$, (c) IrO_2, and (d) FeO_x electrodes.

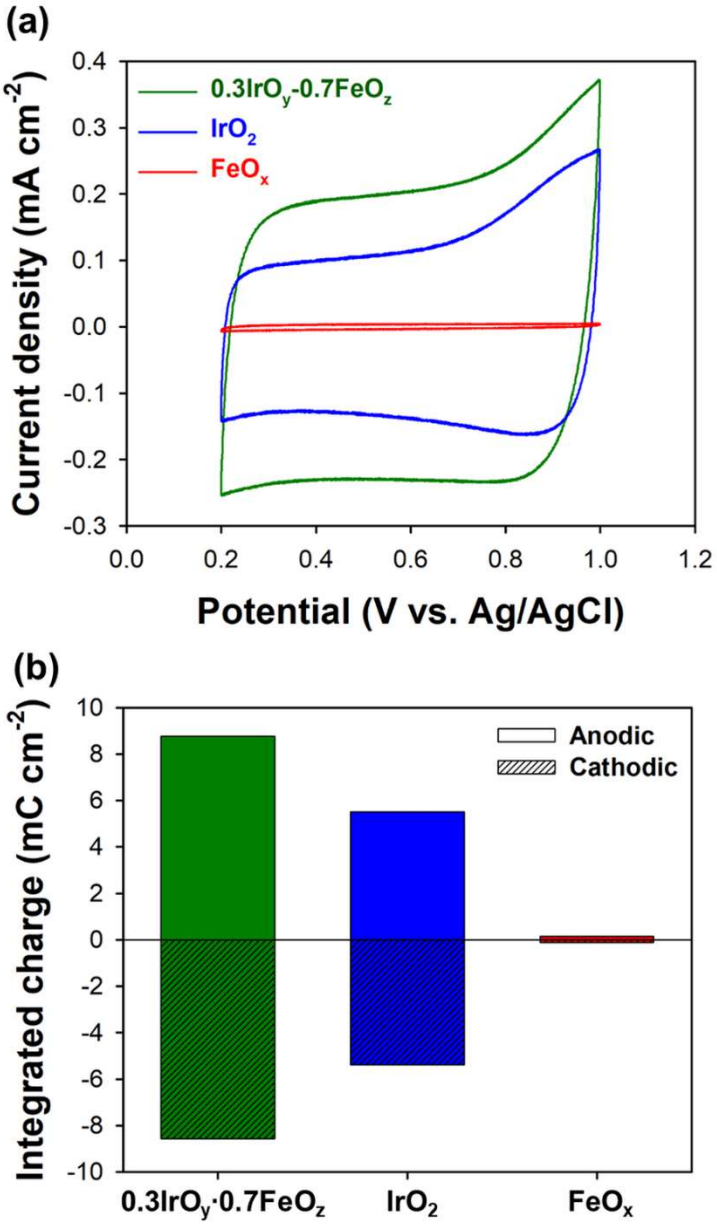

Figure 3-10. (a) Cyclic voltammogram of $0.3IrO_y \cdot 0.7FeO_z$, IrO_2, and FeO_x in 50 mM NaCl (potential range: 0.2 V – 1.0 V, scan rate: 20 mV s^{-1}). (b) Integrated charge of $0.3IrO_y \cdot 0.7FeO_z$, IrO_2, and FeO_x in a cyclic voltammogram.

3.3.7. Chlorine evolution efficiency of the $0.3IrO_y \cdot 0.7FeO_z$ electrode

The performance for CER of the $0.3IrO_y \cdot 0.7FeO_z$ electrode was further investigated at various chloride concentrations (Figure 3-11a). In the dilute Cl^- solution (1 mM to 20 mM NaCl), the current efficiency for CER of $0.3IrO_y \cdot 0.7FeO_z$ (28% – 79%) is much higher than that of IrO_2 (3% – 33%). Furthermore, the $0.3IrO_y \cdot 0.7FeO_z$ electrode exhibits notably higher current efficiency for CER than the other electrodes in concentrated Cl^- solutions as well. It might be attributed to the synergistic effect of and FeO_x (slow reaction rate of the OER) and IrO_2 (fast reaction rate of the CER), which is discussed further below. Prior to the discussion, it should be noted that the simple mixture electrode of FeO_x and IrO_2 exhibited an intermediate value of CER efficiency between that of FeO_x and IrO_2 (Figure 3-11b). This implies that the improvement in CER efficiency of $0.3IrO_y \cdot 0.7FeO_z$ is not only ascribed to simple mixing of FeO_x and IrO_2.

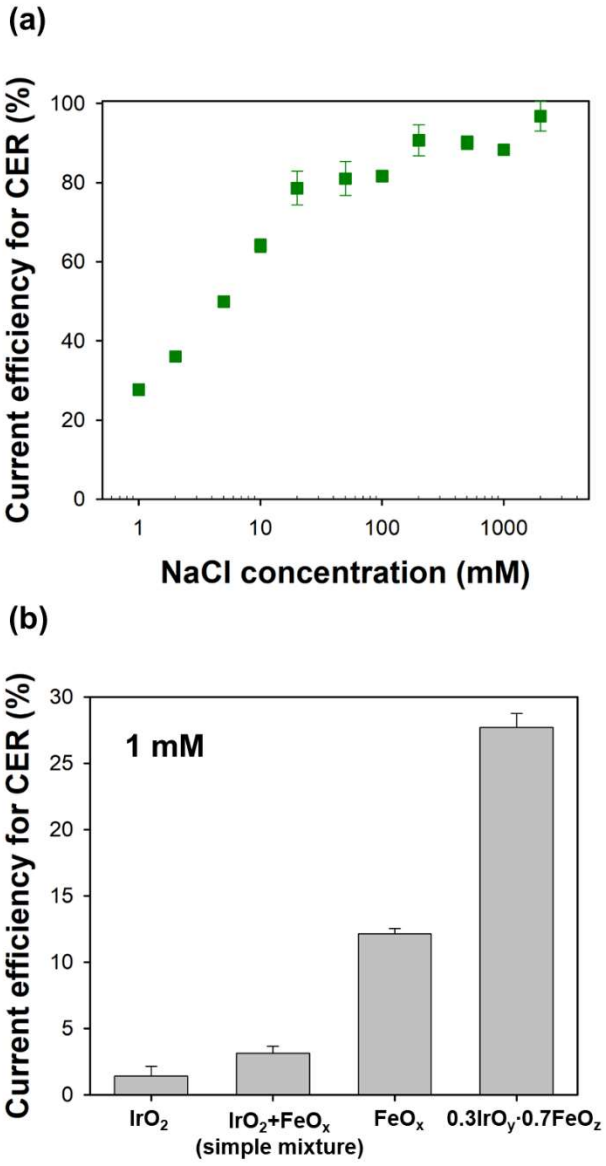

Figure 3-11. Current efficiency for CER of the $0.3IrO_y \cdot 0.7FeO_z$ electrode at various concentrations of NaCl aqueous solution (current density: 10 mA cm^{-2}). Comparison between $0.3IrO_y \cdot 0.7FeO_z$ and simple mixture of IrO_2 and FeO_x (1 mM NaCl).

3.3.8. OER and CER characteristics of the $0.3IrO_y{\cdot}0.7FeO_z$ electrode

To elucidate the efficient electrocatalytic property of $0.3IrO_y{\cdot}0.7FeO_z$ for CER in a dilute Cl^- solution, the OER and CER characteristics of the $0.3IrO_y{\cdot}0.7FeO_z$, IrO_2, and FeO_x were investigated with LSV, EIS, XPS, and volcano curve.

3.3.8.1. Linear sweep voltammetry

Figure 3-12 illustrates the LSV curves of $0.3IrO_y{\cdot}0.7FeO_z$ in concentrated and dilute solutions, respectively. Note that the filled and empty symbols represent the electrolyte in the presence and absence of Cl^-, respectively. As shown in Figure 3-12a, the LSV curve of $0.3IrO_y{\cdot}0.7FeO_z$ in 2 M NaCl revealed a steeper slope and lower overpotential than in 2 M $NaNO_3$. Since CER and OER are dominant reactions in 2 M NaCl and 2 M $NaNO_3$, respectively, $0.3IrO_y{\cdot}0.7FeO_z$ exhibits a higher electrocatalytic activity for CER than OER. The LSV of the $0.3IrO_y{\cdot}0.7FeO_z$ electrode in 2 M NaCl was nearly identical to that of IrO_2 (Figure 3-4). Particularly, in 2 M $NaNO_3$, $0.3IrO_y{\cdot}0.7FeO_z$ reveals lower current density and higher overpotential compared with IrO_2 indicating OER is more suppressed on $0.3IrO_y{\cdot}0.7FeO_z$ than IrO_2. Considering the current flow means reaction kinetics in LSV, it can be assumed that $0.3IrO_y{\cdot}0.7FeO_z$ has fast reaction kinetics for CER with suppressed OER kinetics. In addition, the larger difference between LSV curves in two different solutions implies an improvement of the selectivity for CER because OER is the competitive reaction to CER. It is also verified in the dilute solutions

(Figure 3-12b). As can be seen in Figure 3-12b, $0.3IrO_y \cdot 0.7FeO_z$ shows a similar trend of LSV curves in the dilute solutions with that in the concentration solutions, namely, an evident difference between LSV curves in two different solutions. This means that $0.3IrO_y \cdot 0.7FeO_z$ also exhibits good selectivity for CER in dilute Cl^- solution. The OER suppression on $0.3IrO_y \cdot 0.7FeO_z$ originates from FeO_x component which can be confirmed with LSVs of FeO_x (Figure 3-4). These results suggest that $0.3IrO_y \cdot 0.7FeO_z$ has amphoteric characteristics including FeO_x-like (slow OER kinetics) and IrO_2-like (fast CER kinetics) aspects, resulting in efficient CER behavior.

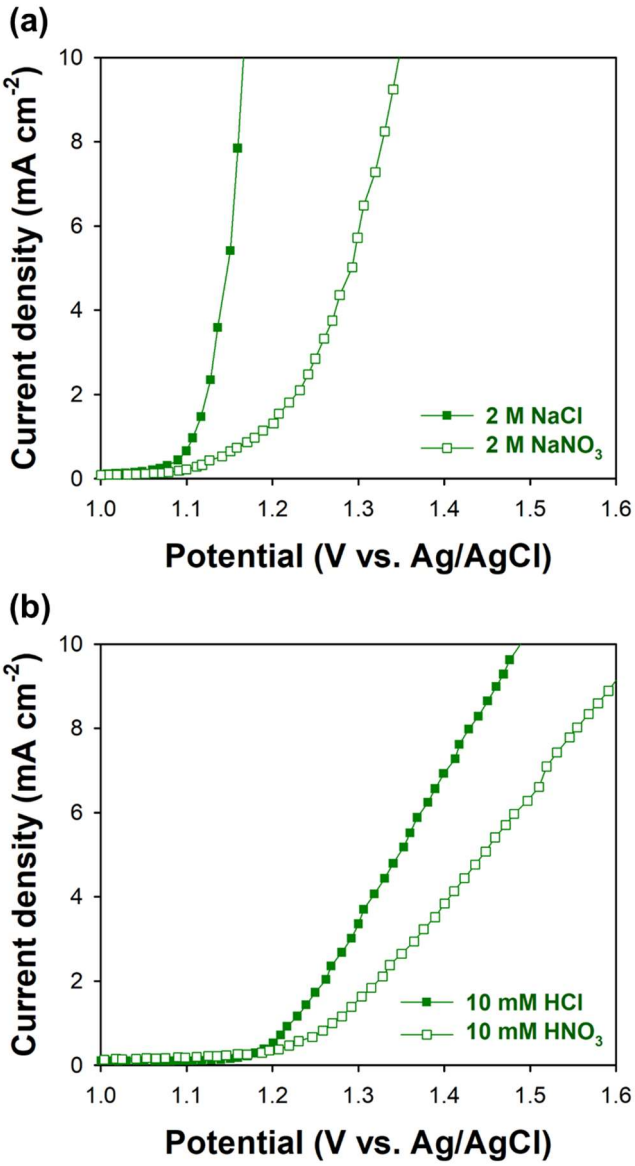

Figure 3-12. Linear sweep voltammograms of the $0.3IrO_y \cdot 0.7FeO_z$ electrode (a) in the highly concentrated aqueous solution (NaCl (2 M) and $NaNO_3$ (2 M)) and (b) in the diluted solutions (HCl (10 mM) and HNO_3 (10 mM)), respectively (scan rate: 2 mV s^{-1}).

3.3.8.2. Charge transfer resistances for CER and OER of the $0.3IrO_y \cdot 0.7FeO_z$ electrode

These amphoteric characteristics of $0.3IrO_y \cdot 0.7FeO_z$ were also supported by EIS analysis (Figure 3-13). Figure 3-13a, b, and c respectively illustrate Nyquist plots of $0.3IrO_y \cdot 0.7FeO_z$, IrO_2, and FeO_x in 2 M NaCl and 2 M $NaNO_3$. From the Nyquist plots, R_{ct} was calculated by fitting a simple Randles circuit and listed in Table 3-2. In 2 M NaCl, $0.3IrO_y \cdot 0.7FeO_z$ showed the same R_{ct} value with IrO_2 of 0.35 Ω. On the other hand, R_{ct} of $0.3IrO_y \cdot 0.7FeO_z$ in 2 M $NaNO_3$ (6.08 Ω) was twice as high as that of IrO_2 (3.06 Ω). As previously stated, the anodic reaction in 2 M NaCl and 2 M $NaNO_3$ can be assumed as CER and OER, respectively. Therefore, it can be concluded that $0.3IrO_y \cdot 0.7FeO_z$ has the same R_{ct} for CER and higher R_{ct} for OER compared with IrO_2, leading to enhancement of CER efficiency. It appears that the high R_{ct} for OER of $0.3IrO_y \cdot 0.7FeO_z$ is attributed to a remarkably high R_{ct} value of FeO_x for OER (2738 Ω). It appears that the high R_{ct} for OER of $0.3IrO_y \cdot 0.7FeO_z$ is attributed to a remarkably high R_{ct} value of FeO_x for OER (2738 Ω).

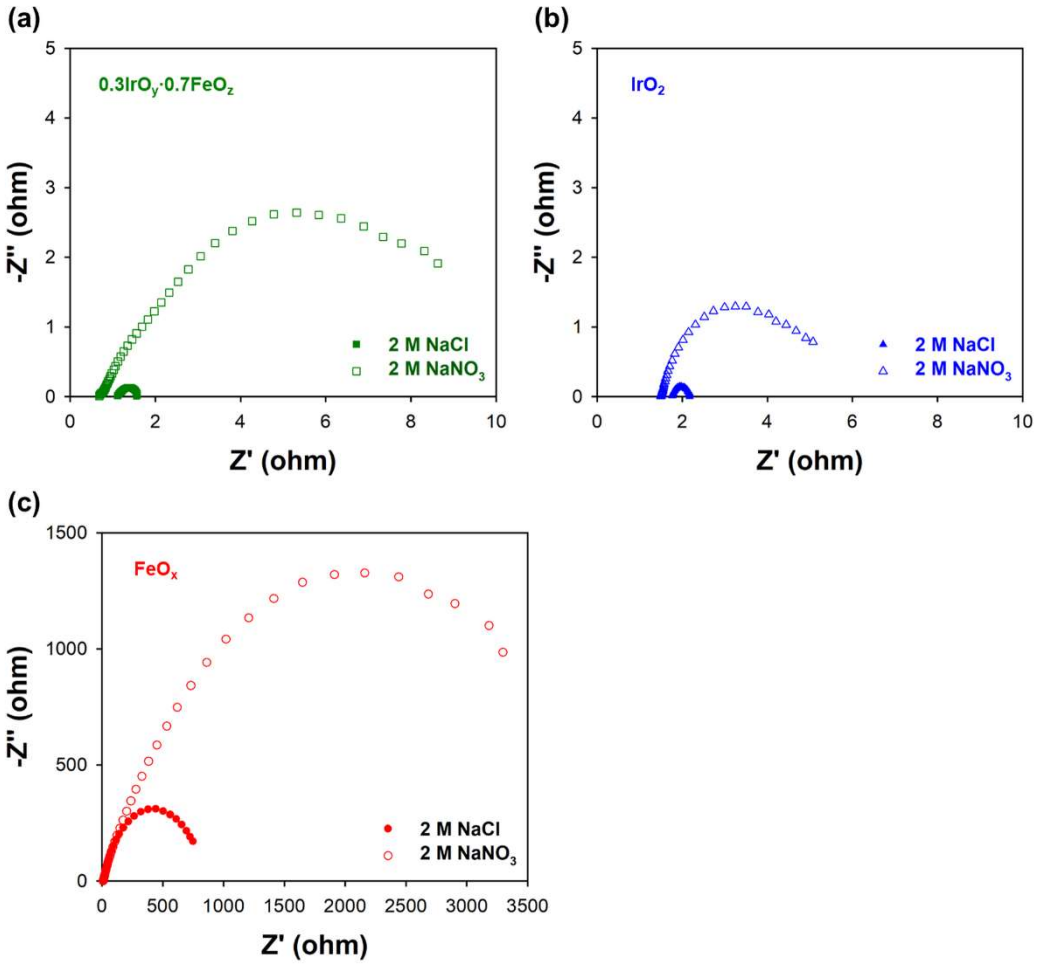

Figure 3-13. Nyquist plots in 2 M NaCl and 2 M $NaNO_3$ of (a) $0.3IrO_y{\cdot}0.7FeO_z$, (b) IrO_2, and (c) FeO_x (at 1.4 V (vs.Ag/AgCl) with 10 mV amplitude, 50 Hz – 50000 Hz).

Table 3-2. R_{ct} values of $0.3IrO_y \cdot 0.7FeO_z$, IrO_2, and FeO_x in 2 M NaCl and 2 M $NaNO_3$.

	R_{ct} (ohm)		
	$0.3IrO_y \cdot 0.7FeO_z$	IrO_2	FeO_x
2 M NaCl	0.35	0.35	659
2 M $NaNO_3$	6.08	3.06	2738

3.3.8.3. XPS analysis

The suppressed OER activity of $0.3IrO_y{\cdot}0.7FeO_z$ is also confirmed by the bonding environments examined by XPS spectra (Figure 3-14). As shown in Figure 3-14a, the peaks for Fe $2p_{1/2}$ and Fe $2p_{3/2}$ are observed in $0.3IrO_y{\cdot}0.7FeO_z$ at 724.6 eV and 711.0 eV, and in FeO_x at 723.8 eV and 710.1 eV, respectively. The peak position of $0.3IrO_y{\cdot}0.7FeO_z$ is positively shifted compared with that of FeO_x. On the other hand, the peaks regarding Ir $4f_{5/2}$ and Ir $4f_{7/2}$ are negatively shifted from 64.9 eV to 64.6 eV and from 61.9 eV to 61.5 eV, respectively, compared with those of IrO_2 (Figure 3-14b). This means that the electron density around the Fe atom is lower in $0.3IrO_y{\cdot}0.7FeO_z$ than in FeO_x, whereas the electron density around the Ir atom is higher in $0.3IrO_y{\cdot}0.7FeO_z$ than in IrO_2. Consequently, the affinity of Fe atoms with negatively charged species becomes stronger in $0.3IrO_y{\cdot}0.7FeO_z$ than in FeO_x, while that of Ir becomes weaker in $0.3IrO_y{\cdot}0.7FeO_z$ than in IrO_2. Therefore, partially negatively charged oxygen atoms (-O, -OH) associated with OER are more easily adsorbed to Fe atoms in $0.3IrO_y{\cdot}0.7FeO_z$, while being less favorable for the adsorption to Ir atoms in $0.3IrO_y{\cdot}0.7FeO_z$ (De Faria, Boodts et al. 1996, Da Silva, Boodts et al. 2001, Hu, Zhang et al. 2004, Grgur and Mijin 2014). Therefore, $0.3IrO_y{\cdot}0.7FeO_z$ exhibits suppressed OER activity similar to FeO_x as Fe atoms in $0.3IrO_y{\cdot}0.7FeO_z$ play a more important role in OER.

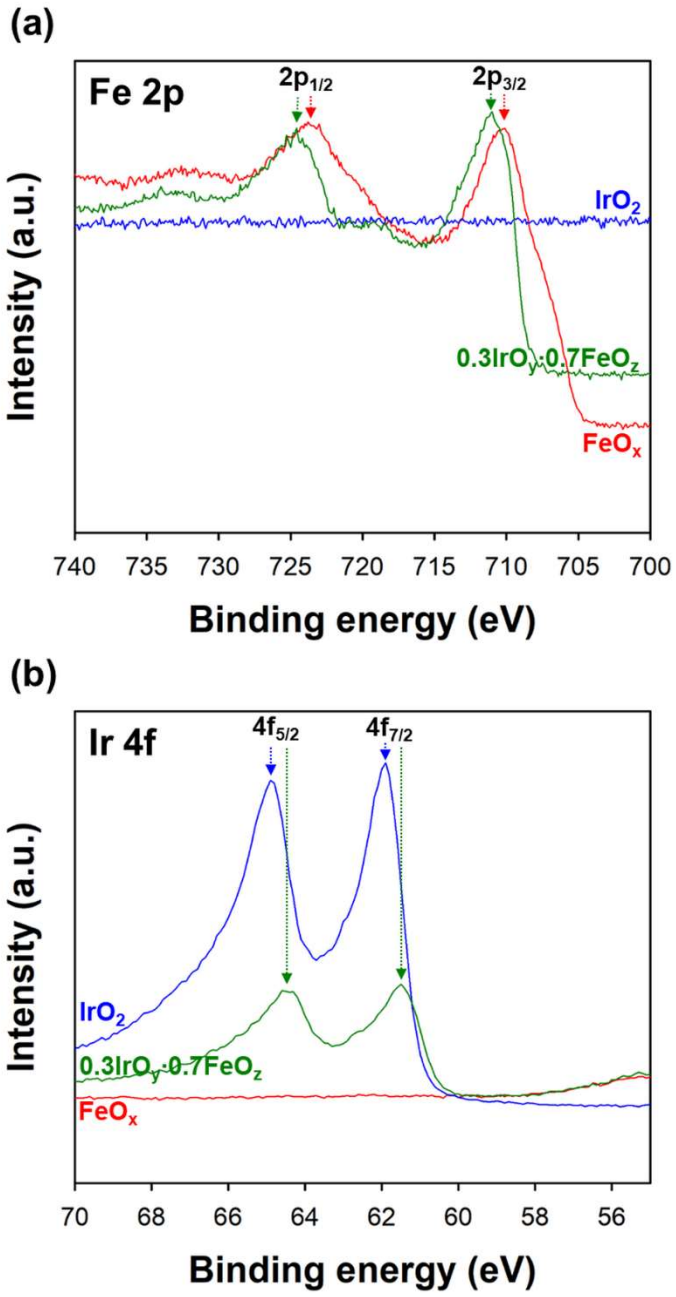

Figure 3-14. XPS spectra of the $0.3IrO_y \cdot 0.7FeO_z$, IrO_2, and FeO_x electrodes with respect to (a) Fe 2p and (b) Ir 4f.

3.3.8.4. Volcano curve of CER

To better understand the electrocatalytic activity of $0.3IrO_y \cdot 0.7FeO_z$ for CER, the volcano curve of CER was obtained with Raman spectroscopy analysis (Figure 3-15). The volcano curve has been frequently used and recognized as an indicator of the activity of the electrode reaction. The volcano curve of CER was proposed by Zeradjanin et al., which correlates the CER activity with the vibration of the Cl−O bond as a dynamic descriptor using Raman spectroscopy. As previously reported (Zeradjanin, Menzel et al. 2012), metal oxides whose Raman shift of the M−O bond is similar to that of Cl−O bond have an optimal catalytic activity for CER. As shown in Figure 3-15**,** the Raman shift of the M−O bond of $0.3IrO_y \cdot 0.7FeO_z$ is very close to the Cl−O bond just like that of IrO_2, implying the $0.3IrO_y \cdot 0.7FeO_z$ also has a good condition for CER. From the LSV, XPS, and Raman spectroscopy analysis, it can be summarized that $0.3IrO_y \cdot 0.7FeO_z$ reveals highly efficient CER behavior resulting from superior CER activity with a suppressed OER activity.

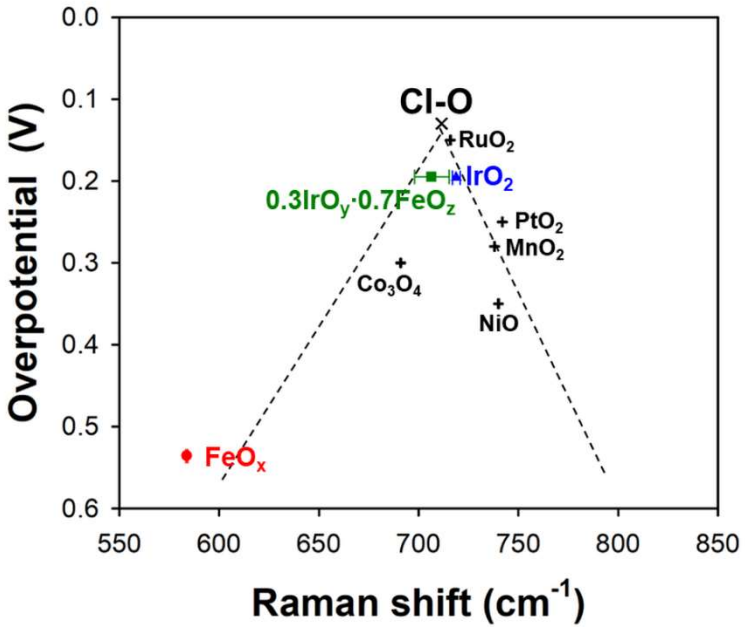

Figure 3-15. Volcano curve of the CER based on the Raman spectroscopy analysis of the $0.3IrO_y{\cdot}0.7FeO_z$ (■), IrO_2 (▲), and FeO_x (●) electrodes and electrochemically produced HClO solution (×) (with IrO_2 in 10 mM NaCl at 10 mA cm^{-2} for 20 min). The values of RuO_2, PtO_2, Co_3O_4, MnO_2, and NiO (+) were taken from the reference (Zeradjanin, Menzel et al. 2012).

3.3.9. Characteristic of the byproducts formation during electrochlorination of the iridium-iron mixed oxide electrodes

To examine the safety of the iridium-iron mixed oxide electrodes, the characteristics of byproduct formation were investigated. Chlorine readily dissolves in water to form hypochlorous acid and hypochlorite as follows:

$$Cl_2 + H_2O \rightarrow HClO + HCl \quad (3\text{-}3)$$

$$HClO \leftrightarrow H^+ + ClO^- \qquad pK_a = 7.54 \text{ at } 25℃ \quad (3\text{-}4)$$

During the electrochlorination, hazardous inorganic byproducts such as chlorite (ClO_2^-), chlorate (ClO_3^-), and perchlorate (ClO_4^-) can be formed as follows (Czarnetzki and Janssen 1992):

$$\text{Chlorite: } HClO + H_2O \rightarrow HClO_2 + 2\,H^+ + 2\,e^- \quad (3\text{-}5)$$

$$ClO^- + 2\,OH^- \rightarrow ClO_2^- + H_2O + 2\,e^- \quad (3\text{-}6)$$

$$\text{Chlorate: } HClO_2 + H_2O \rightarrow ClO_3^- + 3\,H^+ + 2\,e^- \quad (3\text{-}7)$$

$$ClO_2^- + 2\,OH^- \rightarrow ClO_3^- + H_2O + 2\,e^- \quad (3\text{-}8)$$

$$6\,HClO + 3\,H_2O \rightarrow 2\,ClO_3^- + 4\,Cl^- + 12\,H^+ + 3/2\,O_2 + 6\,e^- \quad (3\text{-}9)$$

$$6\,ClO^- + 3\,H_2O \rightarrow 2\,ClO_3^- + 4\,Cl^- + 6\,H^+ + 3/2\,O_2 + 6\,e^- \quad (3\text{-}10)$$

Perchlorate: $ClO_3^- + H_2O \rightarrow ClO_4^- + 2H^+ + 2e^-$ (3-11)

Chlorite can cause methemoglobinemia, hemolysis, kidney failure (Goldfrank, Hoffman et al. 2006). Chlorate is known as a neurotoxin, causing hemolytic anemia by the destruction of red blood cells (Yoon, Cho et al. 2015). In addition, perchlorate has a potent inhibitor of the thyroid sodium-iodide symporter (Braverman, He et al. 2005), and pulmonary toxic effects. Due to the toxicity of the byproducts, WHO suggested through a drinking water guideline that the concentration of chlorite, chlorate, and perchlorate should be below 700 μg L^{-1}, 700 μg L^{-1}, and 15 μg L^{-1}, respectively. Therefore, it is necessary to examine the safety of the electrodes when developing novel electrode materials. The iridium-iron mixed oxide electrodes were examined to confirm the safety for use in practical applications. Figure 3-16 shows the formation of chlorite, chlorate, perchlorate, and chlorine during the electrochlorination from the iridium-iron mixed oxide electrodes at various current densities. Chlorate was the most readily produced byproduct because the rate constant of chlorate formation (Equation (3-7) − (3-8)) is much higher than that of chlorite formation (Equation (3-5) − (3-6)), and the formation of perchlorate (Equation (3-11)) is reported to occur at very high potential and oxygen intermediates should be involved (Czarnetzki and Janssen 1992). The amount of produced chlorate correlates with the amount of produced chlorine. In addition, as the iron component in the iridium-iron mixed oxide electrodes increases, chlorate

tends to be more produced. Iridium-rich mixed oxide electrodes (0 – 11 at.% of Fe) produced chlorite at low current density, and FeO_x also produced chlorite regardless of the current density. Only FeO_x produced the perchlorate, it might be attributed to its high working potential than others.

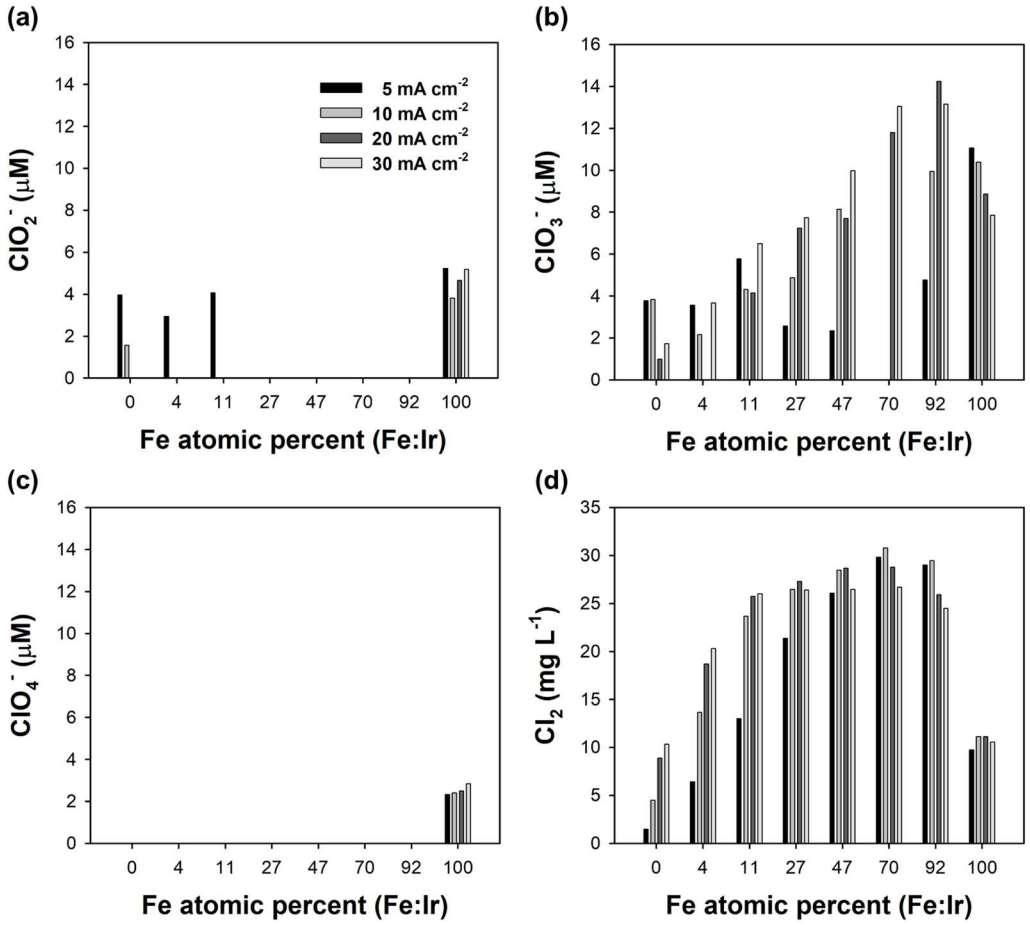

Figure 3-16. Byproducts formation during electrochlorination from the iridium-iron mixed oxide electrodes. The concentration of (a) chlorite, (b) chlorate, (c) perchlorate, and (d) chlorine after the electrochlorination at various current density of 5, 10, 20, and 30 mA cm^{-2} (4 mM NaCl, 30 mL, consumed charge: 5.4 C)

It is necessary to standardize the amount of the produced byproducts regarding the amount of produced chlorine. As the Ministry of Environment of Korea recommends that the concentration of chlorine should be above 0.1 mg L^{-1}, the amount of the produced byproducts was divided by 0.1 mg L^{-1} of chlorine. Therefore, the standardized values of chlorite, chlorate, and perchlorate are 7, 7, and 0.15. Figure 3-17 shows the standardized values of the produced byproducts. After the standardization, the amount of the produced byproducts from the iridium-iron mixed oxide electrodes was much less than the pristine IrO_2 and FeO_x. It is attributed to the much efficient chlorine production from the iridium-iron mixed oxide electrodes compared with the pristine IrO_2 and FeO_x. It was hard to find a distinctive correlation with current density, however, it seems obvious that perchlorate formation is proportional to the working potential (Figure 3-17). It should be noted that the byproducts formation of all electrodes is sufficiently low to satisfy a level of drinking water. In conclusion, the iridium-iron mixed oxide electrodes successfully demonstrated their safety for practical use with a low ratio of byproducts formation.

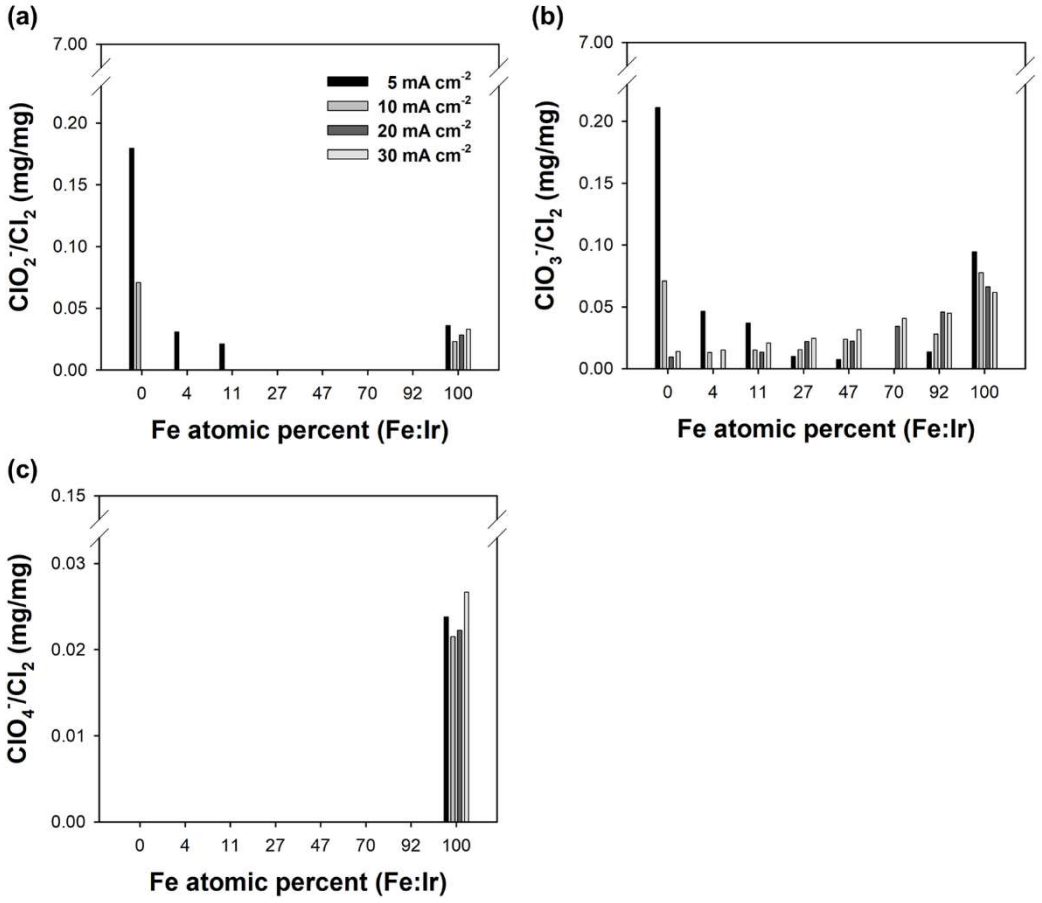

Figure 3-17. Standardized values of the produced (a) chlorite, (b) chlorate, (c) perchlorate divided by 0.1 mg L^{-1} of chlorine. Byproducts formation during electrochlorination from the iridium-iron mixed oxide electrodes at various current density of 5, 10, 20, and 30 mA cm^{-2} (4 mM NaCl, 30 mL, consumed charge: 5.4 C).

3.3.10. Applications of electrochlorination in dilute chloride solutions

3.3.10.1. Arsenite oxidation process

There are several trials to adopt electrochlorination system for arsenite oxidation because it is chemical-free and environmentally benign. However, it turns out to be an inefficient, energy-consuming system because dimensionally stable anodes (IrO_2, RuO_2) for electrochlorination system barely generate chlorine in groundwater-level solution which contains a very low concentration of chloride. Therefore, it is necessary to adopt the anode which can effectively generate chlorine in dilute chloride solutions. Herein, $0.3IrO_y{\cdot}0.7FeO_z$ was used as an electrode in electrochlorination system for arsenite oxidation in groundwater. Figure 3-18 illustrates the arsenite oxidation rate of the $0.3IrO_y{\cdot}0.7FeO_z$, IrO_2, and FeO_x during the electrolysis in the solution with and without chloride. Note that the filled and empty symbols represent the electrolyte in the presence and absence of chloride. In 1 mM NaCl, the $0.3IrO_y{\cdot}0.7FeO_z$ and FeO_x electrodes exhibited much faster oxidation rate compared with chloride-deficient solution (1 mM $NaNO_3$). On the other hand, the arsenite oxidation rate of IrO_2 was nearly identical in NaCl and $NaNO_3$. According to the previous results (Figure 3-3 and 11), electrochlorination in dilute chloride solutions is most efficient with $0.3IrO_y{\cdot}0.7FeO_z$ followed by FeO_x and IrO_2. Therefore, Figure 3-18 implies that arsenite oxidation with chlorine is much effective than direct oxidation or aeration. Arsenite oxidation reaction by chlorine is known as follows (Sorlini and Gialdini 2010):

$$H_3As(III)O_3 + HClO \rightarrow H_2As(V)O_4^- + 2\ H^+ + Cl^- \quad (3\text{-}12)$$

The $0.3IrO_y{\cdot}0.7FeO_z$ electrode completely oxidized 300 μM of arsenite within ten minutes. The efficient CER performance of the $0.3IrO_y{\cdot}0.7FeO_z$ electrode in dilute chloride solutions demonstrated the feasibility of electrochlorination system for the arsenite oxidation process. The effect of chloride concentration was also investigated in Figure 3-19. As the concentration of chloride increases, the arsenic oxidation rate increases. The $0.3IrO_y{\cdot}0.7FeO_z$ electrode showed the most efficient arsenic oxidation followed by FeO_x and IrO_2.

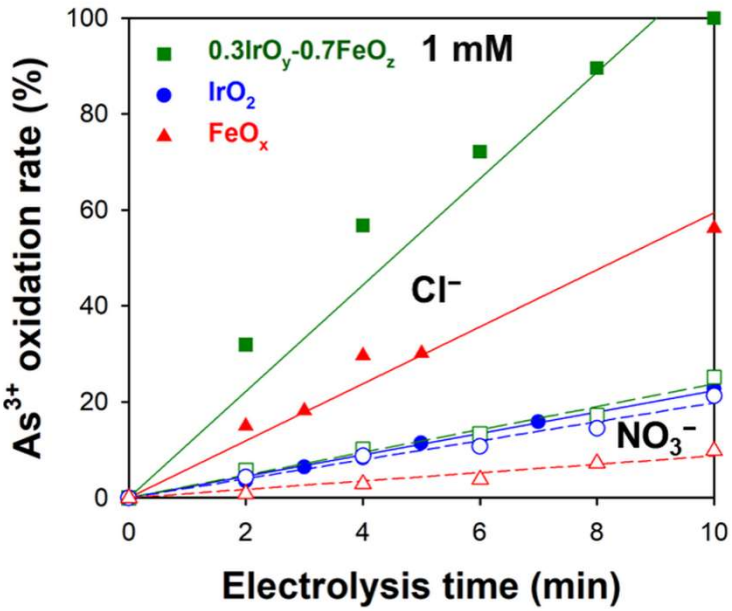

Figure 3-18. Arsenite oxidation during electrolysis in 1 mM NaCl or 1 mM NaCl with $0.3IrO_y{\cdot}0.7FeO_z$, IrO_2, and FeO_x (300 μM NaAs(III)O_2, 10 mA cm^{-2}).

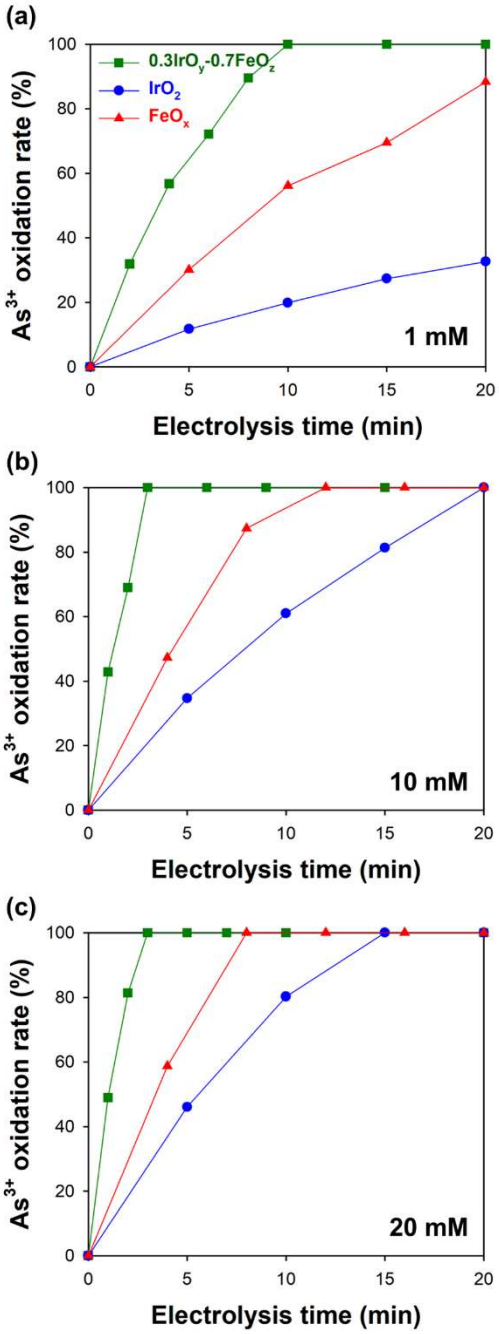

Figure 3-19. Effect of chloride concentration on arsenite oxidation rate (300 μM NaAs(III)O_2 with NaCl, 10 mA cm^{-2}).

3.3.10.2. Ammonium removal

To demonstrate the potential as an anode for electrochlorination in dilute Cl^- solution, an ammonium removal test was conducted in 1 mM NH_4Cl solution (Figure 3-20). The performance for the decomposition of ammonium is in the order of $0.3IrO_y{\cdot}0.7FeO_z > FeO_x > IrO_2$. The $0.3IrO_y{\cdot}0.7FeO_z$ exhibits high effectiveness for ammonium removal in the dilute Cl^- solution, which can be also supported by the pH change resulting from the deprotonation of ammonium with the reaction of Cl_2 into NO_3^- or N_2 (Table 3-3). This is in good agreement with CER efficiency in the dilute Cl^- concentration (Figure 3-3 and 11).

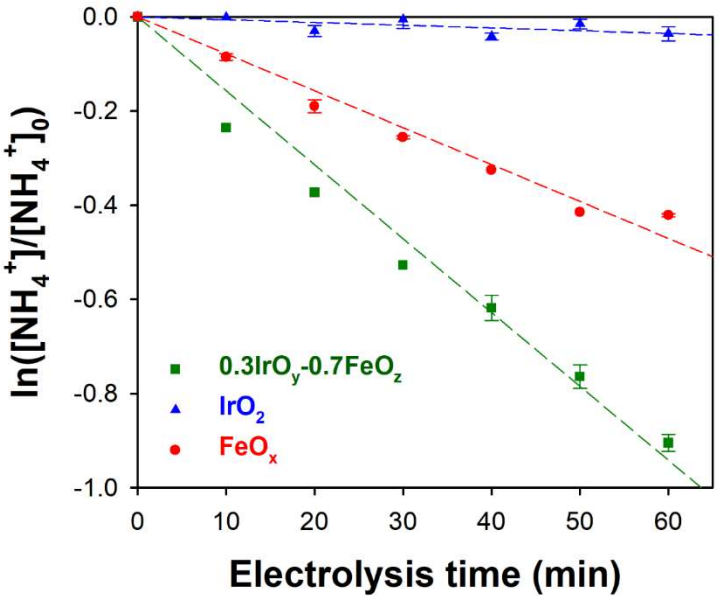

Figure 3-20. Ammonium removal with the $0.3IrO_y{\cdot}0.7FeO_z$, IrO_2, and FeO_x electrodes in a 1 mM NH_4Cl aqueous solution (current density: 10 mA cm^{-2}).

Table 3-3. Changes in the pH after electrochlorination for ammonium removal.

pH	$0.3IrO_y \cdot 0.7FeO_z$	FeO_x	IrO_2
Initial	6.1	6.1	6.1
After electrochlorination	3.5	3.8	6.1

3.3.10.3. Tap water electrolysis

The feasibility of $0.3IrO_y{\cdot}0.7FeO_z$ for practical application in dilute Cl^- solution was assessed with the electrolysis of tap water (Figure 3-21). As can be seen in Figure 3-21a, the concentration of Cl_2 increases from 0.03 mg L^{-1} (residual Cl_2 in tap water) to 6.48 mg L^{-1} with $0.3IrO_y{\cdot}0.7FeO_z$, 1.97 mg L^{-1} with FeO_x, and 1.09 mg L^{-1} with IrO_2, showing that $0.3IrO_y{\cdot}0.7FeO_z$ exhibits the highest CER performance regardless of the presence of other ions. In addition, $0.3IrO_y{\cdot}0.7FeO_z$ requires the lowest energy to produce 1 g of Cl_2 during tap water electrolysis with a value of 0.1 kWh g^{-1}, followed by FeO_x of 0.4 kWh g^{-1}, and IrO_2 of 0.7 kWh g^{-1} (Figure 3-21b). Figure 3-21c shows the voltage profile of the $0.3IrO_y{\cdot}0.7FeO_z$-Pt system during the tap water electrolysis to examine the long-term stability. The $0.3IrO_y{\cdot}0.7FeO_z$ shows notable stability over 50 days although the Cl_2 production rate slightly decreased from 3.47 mg h^{-1} to 2.53 mg h^{-1} due to the partial dissolution of the Fe component (Table 3-4). These results imply that $0.3IrO_y{\cdot}0.7FeO_z$ has a high potential as an electrode for practical applications in dilute water electrochlorination as well as brine electrochlorination.

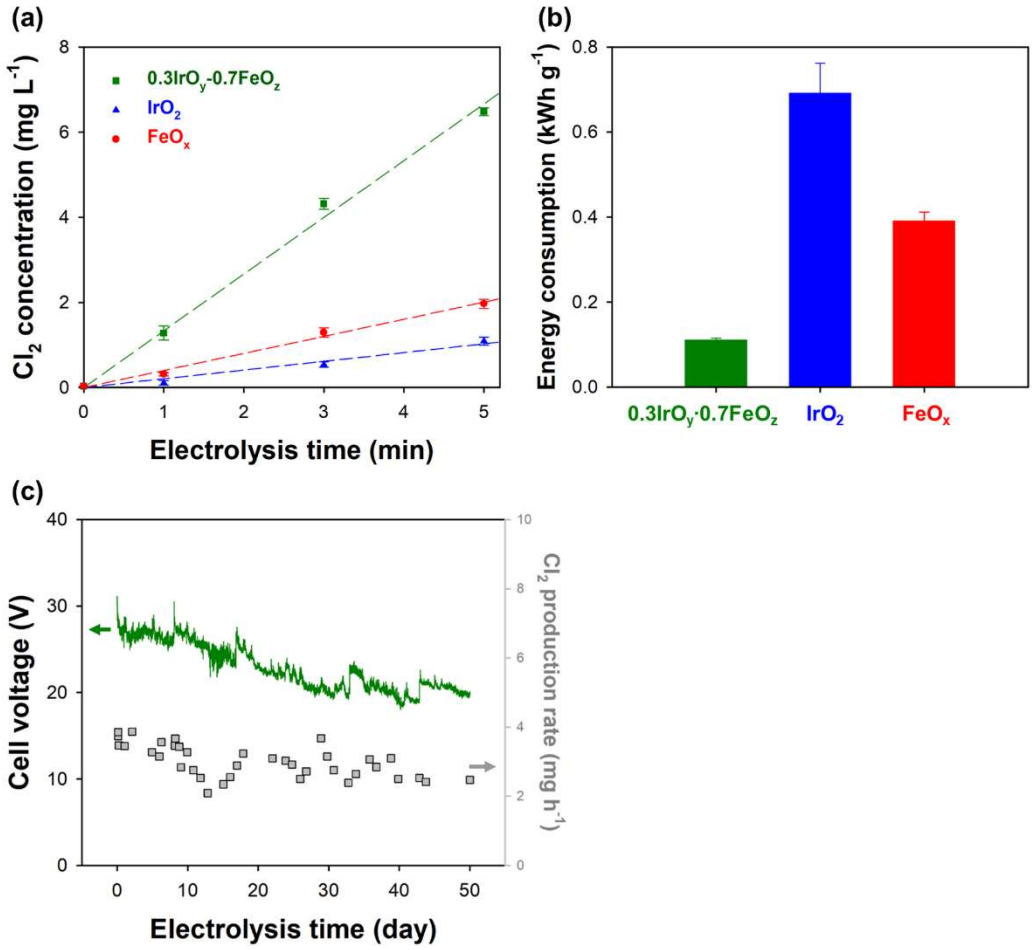

Figure 3-21. Electrochlorination with tap water in Seoul, Korea. (a) Chlorine generation from the $0.3IrO_y{\cdot}0.7FeO_z$, IrO_2, and FeO_x electrodes, and (b) energy consumed to produce 1 g of Cl_2 during tap water electrolysis (current density: 10 mA cm^{-2}). (c) Voltage profile of the $0.3IrO_y{\cdot}0.7FeO_z$–Pt system during the stability test; Cl_2 production rate (mg h^{-1}) before and after the stability test (inset) (current density: 20 mA cm^{-2}).

Table 3-4. EDS analysis of the $0.3IrO_y \cdot 0.7FeO_z$ electrode before and after the stability test.

Atomic ratio (%)	initial	After stability test
Ir	11	13
Fe	25	19
O	64	68

3.4. Summary

The $0.3IrO_y \cdot 0.7FeO_z$ electrode was fabricated to enhance the current efficiency for CER in dilute Cl^- solutions. The $0.3IrO_y \cdot 0.7FeO_z$ exhibited far better current efficiency for CER compared with IrO_2 as a representative of DSA, not only in a dilute Cl^- solution but also in a concentrated Cl^- solution. It is attributed to the synergistic effect originating from amphoteric behavior, including FeO_x-like (slow OER rate) and IrO_2-like (fast CER rate) aspects. The $0.3IrO_y \cdot 0.7FeO_z$ also showed reliable stability during the 50-day operation. In addition, $0.3IrO_y \cdot 0.7FeO_z$ was confirmed to be a safe electrode in respect of the formation of hazardous inorganic byproducts such as chlorite, chlorate, and perchlorate by satisfying a guideline of drinking water. Moreover, the feasibility of $0.3IrO_y \cdot 0.7FeO_z$ for environmental application was successfully proved with arsenite oxidation, ammonium removal, and direct tapwater electrolysis. These results suggest that $0.3IrO_y \cdot 0.7FeO_z$ can be a good alternative to DSA and has the potential to expand the application of electrochlorination systems in dilute Cl^- solutions.

Chapter 4. Iridium-cobalt mixed oxide electrode for efficient chlorine evolution in dilute chloride solutions

4.1. Introduction

Cobalt oxide has the potential to be another candidate for OER suppressor for improving CER efficiency in dilute chloride solutions because the cobalt oxide as well as iron oxide showed relatively higher overpotential for OER than that for CER compared with other electrode materials (Trasatti 1984). In the previous chapter of this study, we investigate with a hypothesis that the material which has a large difference between the overpotential of OER and CER has the potential to enhance the selectivity of CER. To demonstrate the hypothesis and utilize cobalt oxide as another OER suppresser, the iridium-cobalt mixed oxide electrodes were fabricated and examined to confirm the feasibility as another electrode material to enhance the CER efficiency.

4.2. Materials and Methods

4.2.1. Chemicals

All chemicals were reagent grade and used without further purification and were purchased from Sigma-Aldrich Co. All solutions were prepared in deionized water (18.2 MΩ·cm, Milli-Q® Direct 8 system, Merck Millipore, MA, USA).

4.2.2. Preparation of the electrodes

The electrodes were fabricated as anodes with a 1.5 cm^2 (1 cm × 1.5 cm) working area by thermal decomposition and the cathode was the platinum foil of the same size. To fabricate the Co_3O_4 and IrO_2 electrodes, 1.3 g $CoCl_2 \cdot xH_2O$ and 0.8 g $IrCl_3 \cdot xH_2O$ were respectively dissolved in a solvent of 5 mL DI water and 5 mL ethanol as precursor solutions. The iridium-cobalt mixed oxide electrodes ($IrO_a \cdot CoO_b$) were fabricated with various volume percentages (v/v%) of the precursor solutions of Co_3O_4 and IrO_2 (10%, 30%, 50%, 70%, 90%). Titanium foil (Ti) as a substrate was rubbed with sandpaper and etched in 37% HCl solution at 60 °C for an hour. Then, after the substrate was rinsed with DI water and dried, precursor solution (33 μL) was poured onto the substrate and spin-coated using a spin-coater (Model WS-400BZ-6NPP/Lite, Laurell Technologies Co., PA, USA) for 15 s at 100 rpm. To evaporate the solvent, electrodes were dried at 100 °C for 5 min and annealed at 500 °C for 5 min. These spin-coating and annealing processes were repeated four times. After these processes, the electrodes were annealed at 500 °C for 5 h under atmospheric conditions.

4.2.3. Characterization of the electrodes

The surfaces and chemical compositions of the $IrO_a \cdot CoO_b$, Co_3O_4, and IrO_2, electrodes were characterized by field-emission scanning electron microscopy (FE-SEM) coupled with an energy-dispersive X-ray spectroscopy (EDS) system (JSM-7800F Prime, JEOL). The crystal structure and elemental composition were analyzed by X-ray diffraction (XRD; SmartLab, Rigaku) with Cu Kα radiation (40 kV, 250 mA) in the 2θ range of 10° – 80° at a scan rate of 2° s^{-1} and X-ray photoelectron spectroscopy (XPS; Sigma probe, Thermo). The photoelectron spectra were excited by an Al Kα (1486.6 eV) anode operating at a constant power of 150 W (15 kV and 10 mA). Raman spectroscopy measurements were conducted with a confocal Raman microscope (LabRam 300, JY-Horiba) equipped with a thermoelectrically cooled charge-coupled device (CCD) detector. The 660 nm laser line from a diode-pumped solid-state laser (Cobolt Flamenco, Sweden) was used for excitation sources.

4.2.4. Electrochemical measurements

The electrochemical properties of anodes were measured by cyclic voltammetry (CV), linear sweep voltammetry (LSV), and electrochemical impedance spectroscopy (EIS) using a three-electrode system with Ag/AgCl (KCL sat.). EIS was conducted using a potentiostat (VersaSTAT 3, Princeton Applied Research) and the rest of the electrochemical experiments were performed using a battery cycler (WBC3000, WonATech). CV was performed at a scan rate of 20 mV s^{-1} in the potential range of 0.2 V – 1.0 V (vs. Ag/AgCl) in 50 mM NaCl electrolyte. LSV was performed at a scan rate of 2 mV s^{-1} in the potential range of 1.0 V – 1.6 V (vs. Ag/AgCl). To figure out OER and CER onset potential with chloride concentration, 2M of NaCl, $NaNO_3$, and 10mM of HCl, HNO_3 aqueous solutions were used respectively. Because it is not easy to distinguish CER and OER onset potential in dilute aqueous solutions, 10mM of HCl and HNO_3 aqueous solutions were used to suppress the OER in acidic conditions. To measure charge transfer resistance (R_{ct}) for CER and OER, EIS data was recorded at 1.3 V (vs. Ag/AgCl) for 10 mV amplitude with a frequency region of 10 Hz – 100,000 Hz in 1M NaCl and 1M $NaNO_3$.

4.2.4.1. Evaluation of CER efficiency

Chlorine evolution reaction (CER) efficiency for $IrO_a{\cdot}CoO_b$, Co_3O_4, and IrO_2 electrodes were measured in a current density of 10 mA cm^{-2} in a 30 mL NaCl

aqueous solution with a stirring rate of 200 rpm. The free chlorine concentration in bulk was measure at 5 minutes using N,N-diethyl-p-phenylenediamine (DPD) method at 530 nm with a spectrophotometer (DR 900, HACH Co., USA). The current efficiency for CER was calculated by Equation (4-1):

$$\text{Current efficiency for CER (\%)} = (C \cdot V \cdot n \cdot F) / (j \cdot A \cdot t) \times 100 \quad (4\text{-}1)$$

, where C is the concentration of free chlorine (mol L^{-1}), V is working volume (L), n is the number of electron transfer (2 eq mol^{-1}), F is the Faraday constant (96485 C mol^{-1}), I is the applied current (A), and t is the electrolysis time (s).

4.2.4.2. Accelerated stability test

Accelerated stability test (AST) was performed in 0.5 M H_2SO_4 solution at a current density of 0.1 A cm^{-2}. After AST, the chemical compositions of $IrO_a \cdot CoO_b$ electrode were measured by an energy-dispersive X-ray spectroscopy (EDS) system.

4.2.4.3. Ammonium degradation test

To better understand the feasibility of the $IrO_a \cdot CoO_b$ for the application of real wastewater treatment (Hong, Chan et al. 2007, Fontenot, Lee et al. 2013), the ammonium degradation test was performed in a volume of 30 mL containing 2 mM

of ammonium and 15 mM of chloride at 10 mA cm^{-2} for 1 h. Ammonium ions were measured by ion chromatography (ICS-1100, Thermo Fisher Scientific Inc).

4.3. Results and Discussion

4.3.1. Cobalt oxide as another candidate material for suppressing oxygen evolution reaction

Figure 4-1a shows the onset potential for CER against that for OER of various electrode materials. In accordance with the previous research (Trasatti 1984), the cobalt oxide as well as iron oxide showed relatively higher overpotential for OER than that for CER compared with other electrode materials. At the very first of this study, we investigate with a hypothesis that the material which has a large difference between the overpotential of OER and CER has the potential to enhance the selectivity of CER. To demonstrate the hypothesis and utilize cobalt oxide as another OER suppresser, the current efficiency for CER in 1 mM NaCl of various electrodes was compared in Figure 4-1b. Although iron oxide showed the highest CER efficiency, cobalt oxide also showed highly efficient CER performance compared with MnO_2, IrO_2, and RuO_2. As cobalt oxide exhibited much lower CER overpotential than iron oxide, cobalt oxide has the potential as a highly active CER catalyst as well as an efficient OER suppressor. To examine the feasibility of cobalt oxide as an efficient CER catalyst, we fabricated iridium-cobalt mixed oxide electrodes just as we fabricate the iridium-iron mixed oxide electrodes.

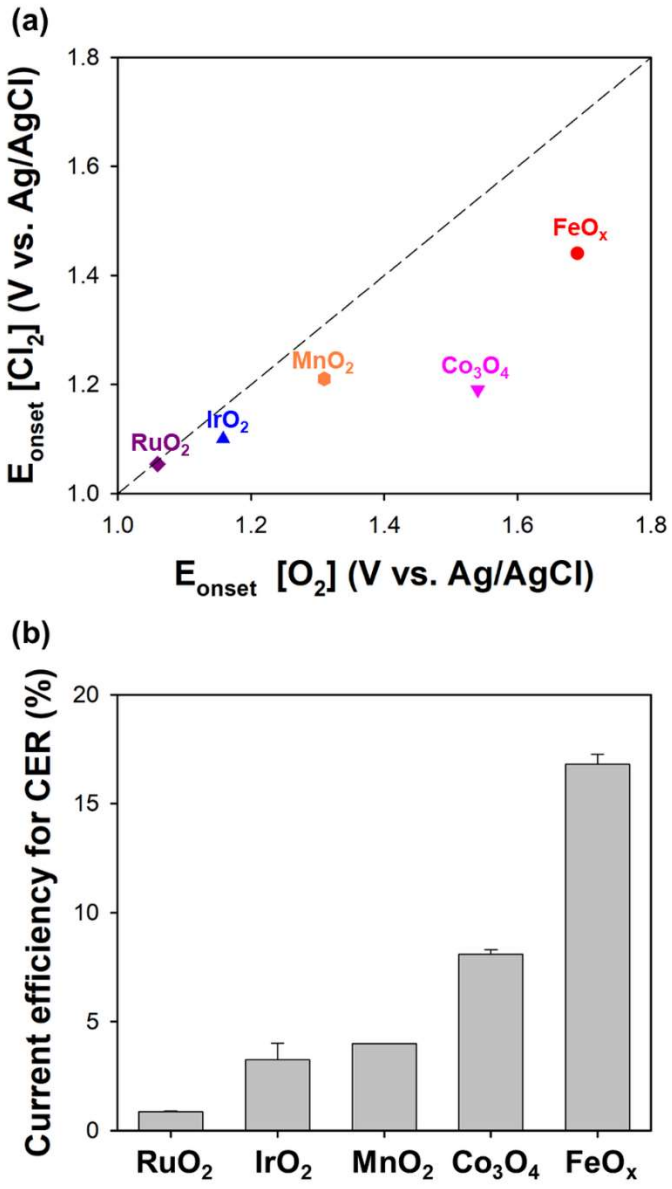

Figure 4-1. (a) Onset potential for chlorine evolution reaction against that oxygen evolution reaction of various metal oxides (2 M NaCl, 2 M $NaNO_3$, current density: 0.5 mA cm^{-2}). (b) current efficiency for CER of various electrode materials in 1 mM NaCl (current density: 10 mA cm^{-2}).

4.3.2. Selection of the representative iridium-cobalt mixed oxide electrode

Figure 4-2 shows the current efficiency for CER of the iridium-cobalt mixed oxide electrodes with various compositions in 1 mM NaCl at 10 mA cm^{-2}. Among the iridium-cobalt mixed oxide electrodes, the electrode made with 90 v/v% of $CoCl_2$ precursor solution showed the highest CER current efficiency. We selected the electrode and denote it as ICO for further experiment to investigate CER performance and electrochemical property.

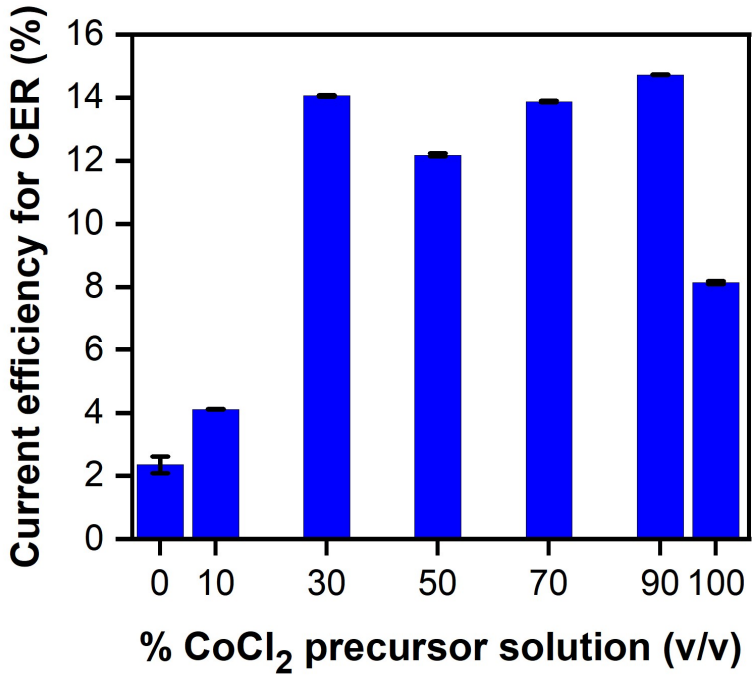

Figure 4-2. Current efficiency for CER of the iridium-cobalt mixed oxide electrodes with various volume percentages (v/v%) of the IrO_2 and $CoCl_2$ precursor solutions (1 mM NaCl, current density: 10 mA cm^{-2}).

4.3.3. The characterization of the iridium-cobalt mixed oxide electrode

Figure 4-3 shows the XRD patterns and SEM images of ICO, Co_3O_4, and IrO_2 electrodes. Figure 4-3a illustrates XRD patterns for as prepared ICO, mainly involving the peaks of IrO_2, and Co_3O_4 electrodes (JCPDS PDF# 74-1656, 86-0330). As shown in the SEM images of Co_3O_4 and IrO_2 (Figure 4-3c and d), the particle size of Co_3O_4 is far bigger than IrO_2. The relatively small IrO_2 particles are well distributed to Co_3O_4 particles in ICO (Figure 4-3b). It is supported by EDS mapping (Figure 4-4). This structural character may lead to ICO's larger electroactive surface area than IrO_2 and Co_3O_4, which is supported by CV test (Figure 4-5). The integrated charges in the anodic and cathodic current of electrodes are described in Table 4-1. Although the integrated charge of Co_3O_4 is about six times smaller than that of IrO_2, ICO shows the largest electrochemically active surface area which might lead to high CER performance. Quantitative analysis was conducted with EDS (Table 4-2).

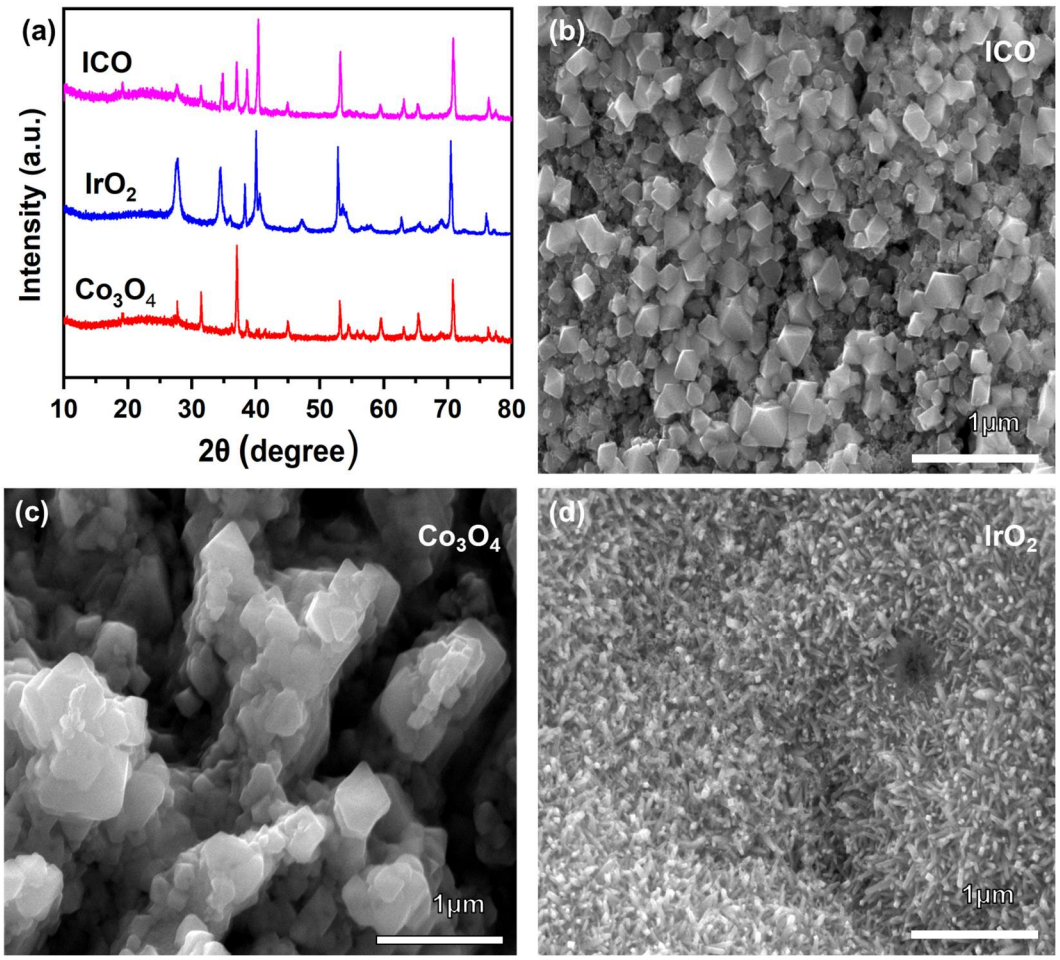

Figure 4-3. (a) XRD patterns of ICO, IrO_2, and Co_3O_4 electrodes. SEM images of the (b) ICO, (c) Co_3O_4, and (d) IrO_2 electrodes.

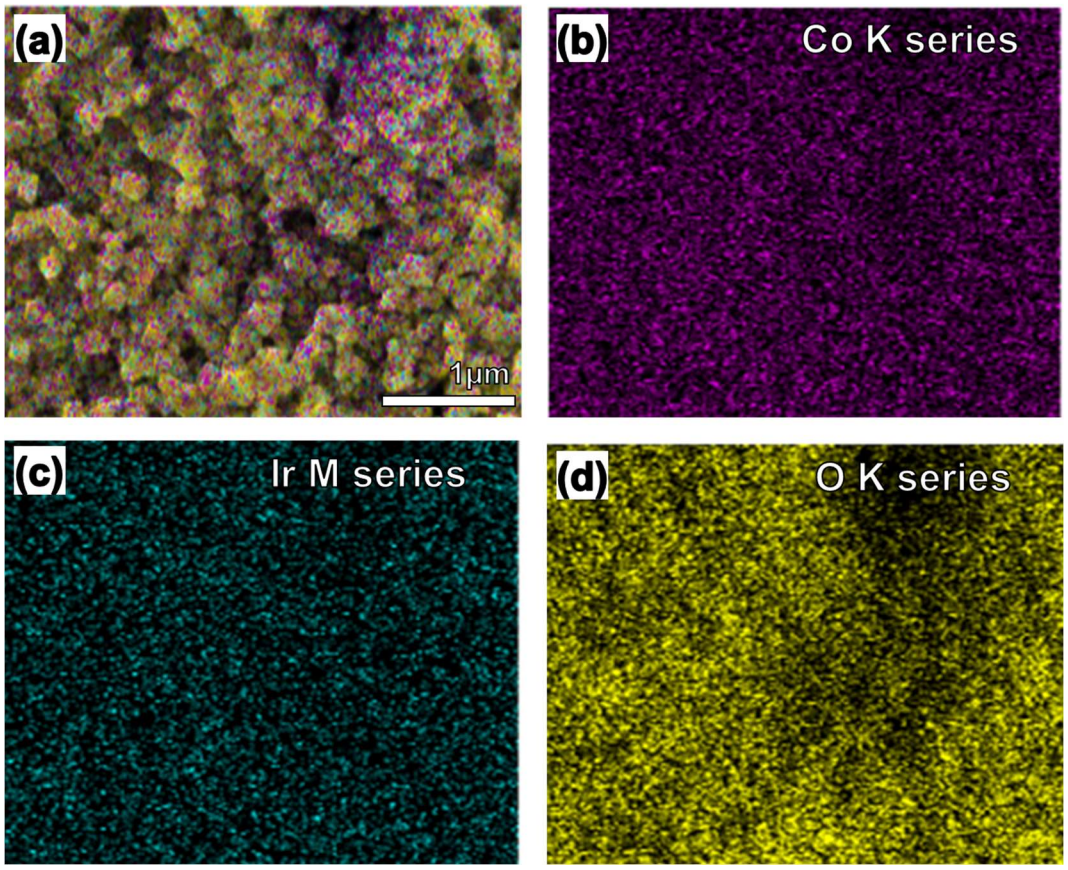

Figure 4-4. EDS data of ICO electrode: (a) EDS layered FE-SEM image, and EDS maps of (b) Co, (c) Ir, and (d) O.

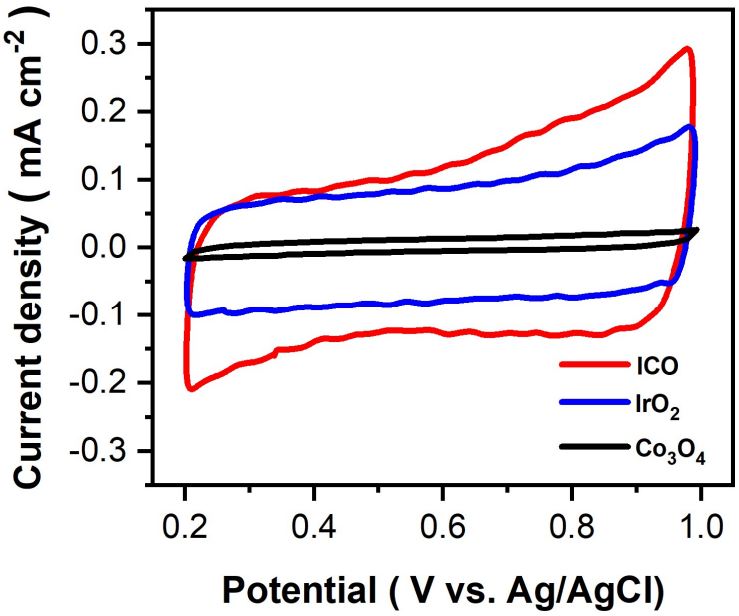

Figure 4-5. Cyclic voltammograms of ICO, IrO_2, and Co_3O_4 in 50 mM NaCl (potential range: 0.2 − 1.0 V vs Ag/AgCl, scan rate: 20 mV s^{-1}).

Table 4-1. Integrated charge of ICO, IrO_2, and Co_3O_4 electrodes in cyclic voltammograms (potential range: 0.2 – 1.0 V vs Ag/AgCl, scan rate: 20 mV s^{-1}).

Integrated Charge (mC cm^{-2})	ICO	IrO_2	Co_3O_4
Anodic Current	5.6	3.9	0.6
Cathodic current	5.3	3.1	0.3

Table 4-2. Atomic ratio (%) of ICO electrode form EDS data.

Element	Atomic ratio (%)
Ir	2
Co	46
O	52

4.3.4. CER efficiency of the iridium-cobalt mixed oxide electrode

Figure 4-6 shows CER current efficiency and energy consumption of the ICO, Co_3O_4, and IrO_2 electrodes. As shown in Figure 4-6a, The ICO shows excellent CER performance compared with Co_3O_4 and IrO_2. In the dilute chloride solution (1 mM NaCl), the current efficiency of CER on ICO was approximately 15%, which is a 7-fold improvement compared to IrO_2 (2%). Besides, the CER efficiency of ICO was better than that of Co_3O_4 (8%). In particular, above 50 mM NaCl concentration, the ICO exhibits an excellent CER efficiency close to unity. In addition, even in the high concentration of chloride solution (0.1 M − 2 M NaCl), we see the ICO has higher CER efficiency compared with IrO_2. Accordingly, the ICO electrode shows the smallest energy consumption for CER (Figure 4-6b). The energy consumption for generating 1 g of chlorine on the ICO electrode is about 10.3 Wh g^{-1} in 10 mM NaCl at 10 mA cm^{-2}, whereas the IrO_2 electrode consumed about 42.4 Wh g^{-1}. These results indicate the ICO has great potential as an optimum CER anode for its high CER performance with low energy consumption.

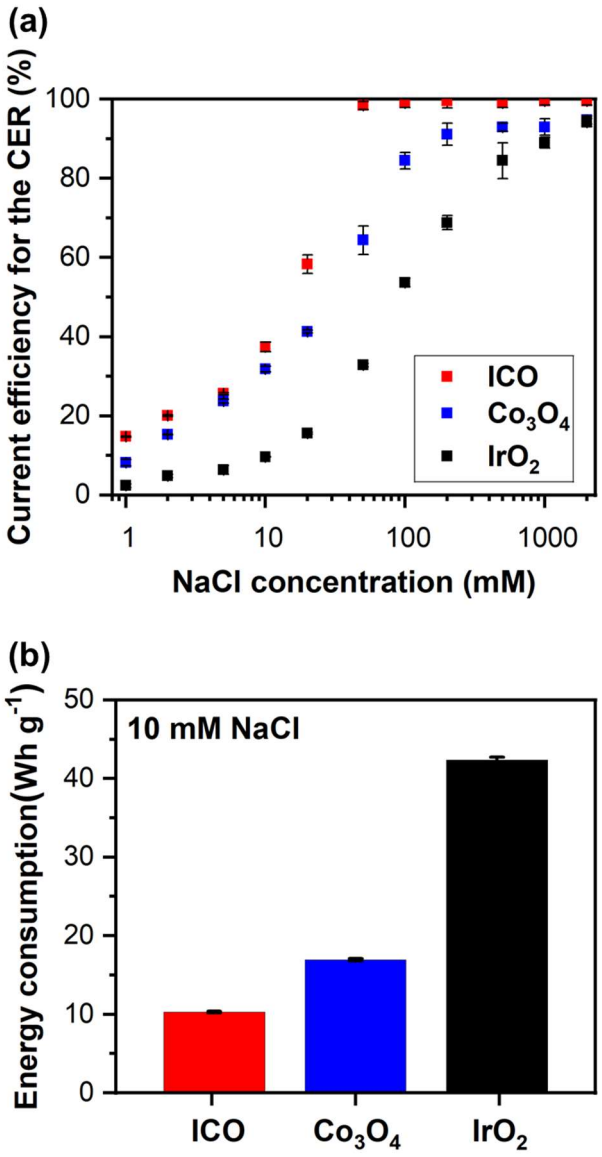

Figure 4-6. (a) CER Current efficiency of the ICO, Co_3O_4, and IrO_2 electrodes in various concentrations of NaCl aqueous solutions (current density: 10 mA cm^{-2}). (b) CER energy consumption of ICO, Co_3O_4, and IrO_2 electrodes (10 mM NaCl, current density: 10 mA cm^{-2}).

4.3.5. Characteristics of CER and OER of the iridium-cobalt mixed oxide electrode

The electrocatalytic activity for CER and OER of the ICO, IrO_2, and Co_3O_4 electrodes was compared via LSV curves in concentrated solutions and dilute solutions (Figure 4-7). As CER and OER are predominant in concentrated NaCl and $NaNO_3$ solutions, respectively, the current flow in 2 M NaCl and 2 M $NaNO_3$ can be approximated as CER and OER. As shown in Figure 4-7a, the ICO shows slightly higher CER activity and lower OER activity compared with IrO_2. Interestingly, in dilute solutions (Figure 4-7b), the difference in LSV curves between ICO and IrO_2 becomes more distinct. The ICO shows an evident difference between LSV curves for CER and OER with 37 mV of the onset potential gap whereas the difference on IrO_2 was negligible (Note that the onset potential was defined as the potential at a current density of 2 mA cm^{-2}). Since the current flow refers to reaction rate in LSV, it can be assumed that ICO exhibits a faster CER rate with a lower OER rate compared to IrO_2. Furthermore, the larger difference between LSV curves in two different solutions implies an improvement of the selectivity for CER because OER is the competitive reaction to CER. Considering the Co_3O_4 shows large onset potential differences of 290 mV and 48 mV in concentrated and dilute solution, respectively (Figure 4-8a and b). it can be concluded that cobalt oxide components lead to the improvement in CER selectivity.

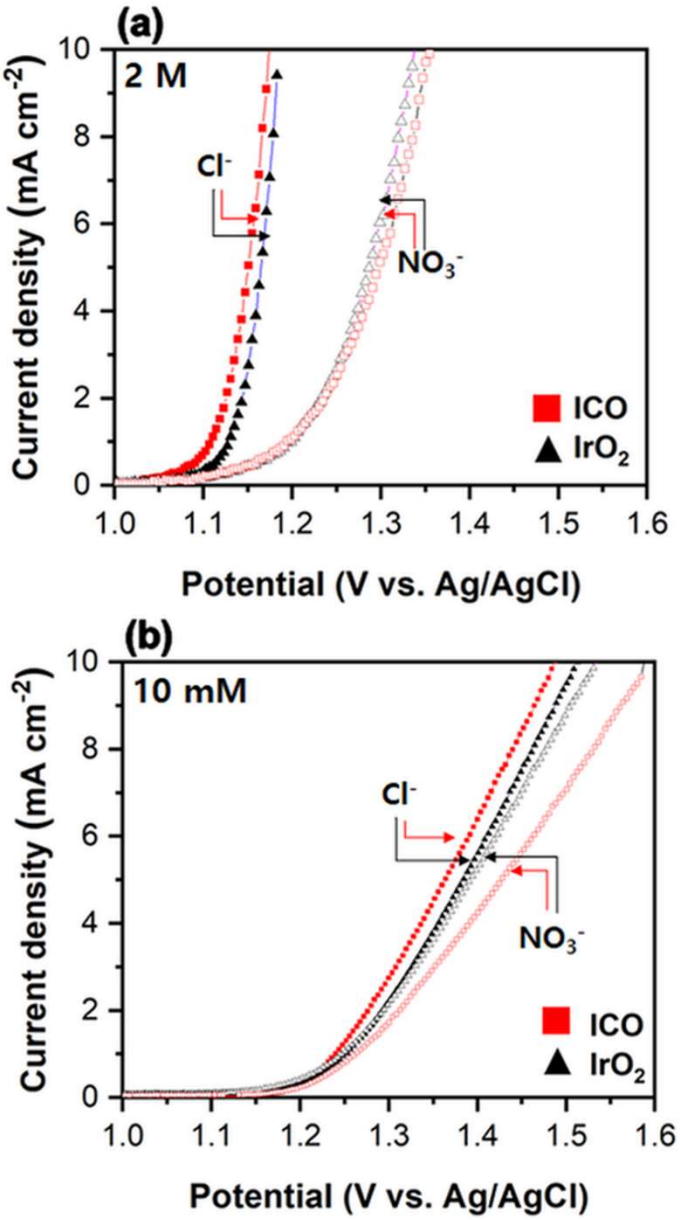

Figure 4-7. LSV curves of ICO and IrO_2 electrodes in (a) concentrated aqueous solutions (2 M NaCl, 2 M $NaNO_3$) and (b) dilute solutions (10 mM HCl, 10 mM HNO_3), respectively (scan range: 1.0 − 1.6 V vs Ag/AgCl, scan rate: 2 mV s^{-1}).

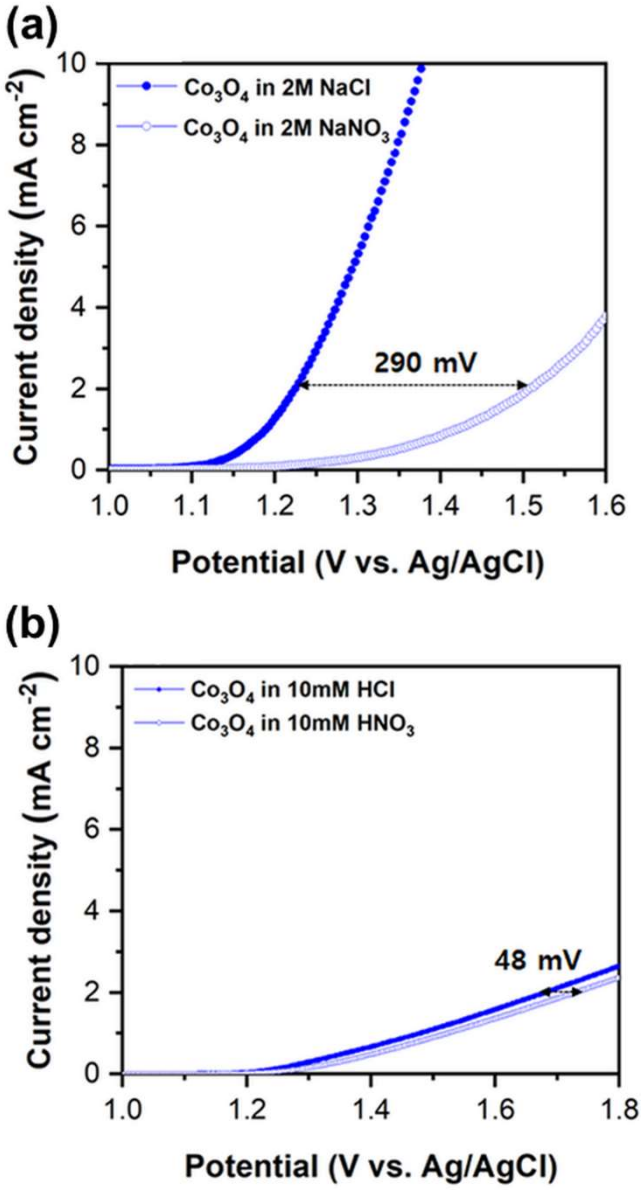

Figure 4-8. LSV curve of Co_3O_4 electrode in (a) concentrated aqueous solutions (2 M NaCl, 2 M $NaNO_3$) and (b) dilute solutions (10 mM HCl, 10 mM HNO_3), respectively (scan range: 1.0 − 1.6 V vs Ag/AgCl, scan rate: 2 mV s^{-1}).

4.3.6. Charge transfer resistance of CER and OER of the iridium-cobalt mixed oxide electrode

The electrocatalytic activity of ICO for CER and OER is also supported by EIS analysis. Figure 4-9 illustrates Nyquist plots of ICO, IrO_2, and Co_3O_4 in 1 M NaCl and 1 M $NaNO_3$. Charge transfer resistance (R_{ct}) was analyzed by fitting to Randles circuit model and listed in Table 4-3. It is reasonable to assume that the R_{ct} values measured in 1 M NaCl and $NaNO_3$ solutions refer to charge transfer resistance for CER and OER, respectively because the current efficiency for CER of ICO and IrO_2 are above 90% in 1M NaCl solution. R_{ct} value of ICO in NaCl (0.1 Ω) is about ten times lower than IrO_2 in NaCl (1.1 Ω), which contributes to ICO's superior CER current efficiency and low energy consumption. In addition, considering the R_{ct} ratio between OER and CER ($R_{ct,OER}$ / $R_{ct,CER}$) of ICO (about 56) is far greater than that of IrO_2 (about 5), it can be concluded that ICO has more CER selectivity than IrO_2, which is in good agreement with LSV test.

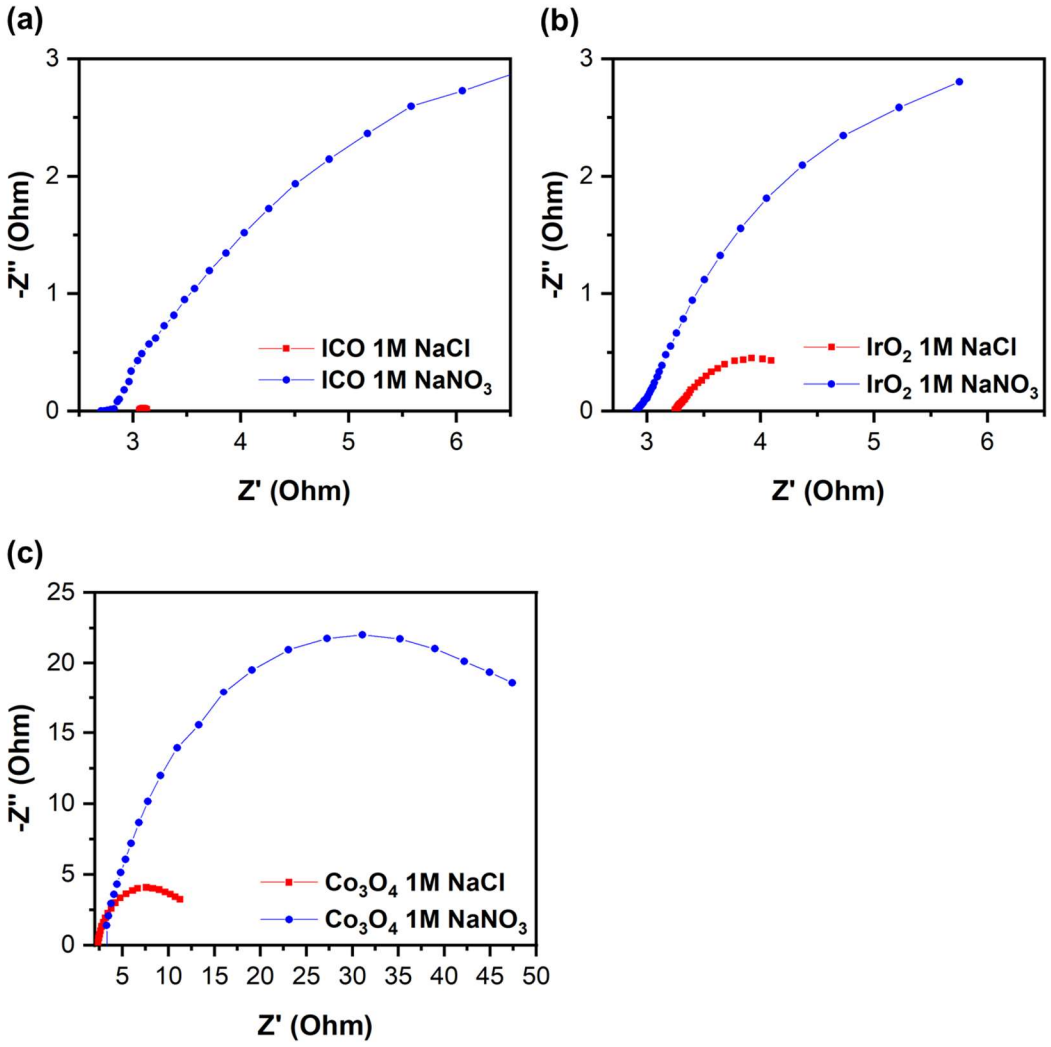

Figure 4-9. Nyquist plots in 1 M NaCl and 1M $NaNO_3$ of (a) ICO and (b) IrO_2 electrodes (at 1.3 V vs Ag/AgCl with 10 mV amplitude, 10 Hz − 100,000 Hz).

Table 4-3. R_{ct} (Ω) values of ICO, IrO_2, and Co_3O_4 electrodes in 1 M NaCl and 1M $NaNO_3$.

Solution	R_{ct} (ohm)		
	ICO	IrO_2	Co_3O_4
1M NaCl	0.1	1.1	7.9
1M $NaNO_3$	5.6	5.1	44.0

4.3.7. Volcano curve of CER

The high electrocatalytic activity of ICO can be explained by the vibration frequency of crystal lattice (M−O). As can be seen in Figure 4-10a, the Raman shifts of M−O were 692, 714, and 723 cm^{-1} at Co_3O_4, ICO, and IrO_2, respectively (The Raman spectra are shown in Figure 4-10b (Zeradjanin, Menzel et al. 2012, Kim, Kim et al. 2015). It is attributed to that the intermediate during the CER is easily formed and cleaved when the vibrational frequency of M−O is in resonance with that of Cl−O. Thus, a similar vibration frequency of M−O in ICO and Cl−O can allow high CER activity. This is also well supported by a high CER efficiency of IrO_2-Fe_2O_3 in dilute Cl^- solution (charge efficiency of 80% in 50 mM NaCl solution) and the Raman shift (706 cm^{-1}) of which is close to the vibration frequency of Cl−O originating from the synergistic effect of the mixture of Fe_2O_3 and IrO_2.

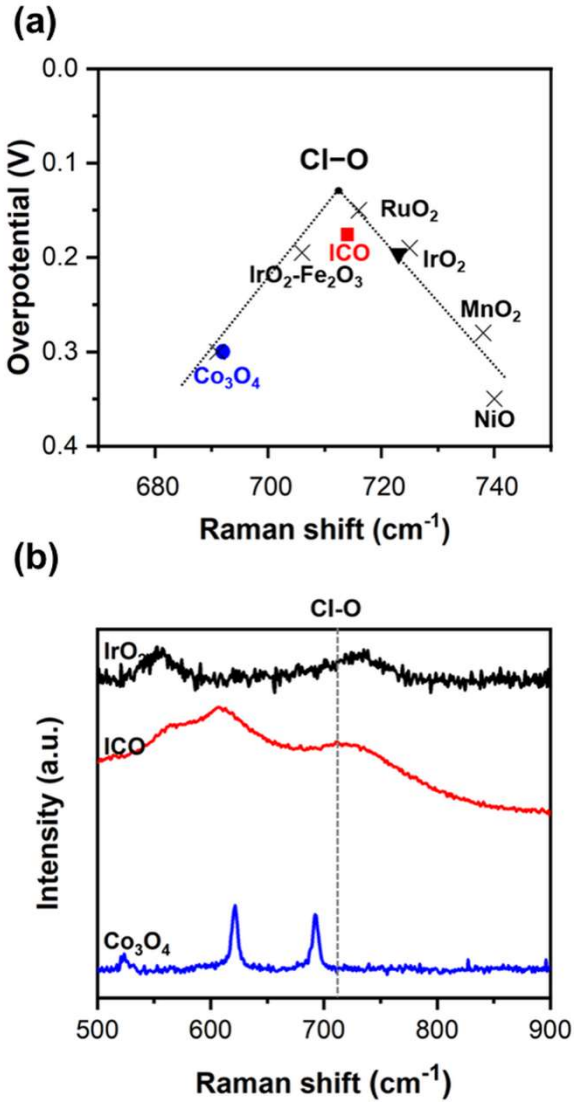

Figure 4-10. (a) Volcano curve of the CER based on the Raman spectroscopy analysis of the ICO (■), IrO_2 (▼), and Co_3O_4 (●) electrodes. The values of RuO_2, PtO_2, Co_3O_4, MnO_2, and NiO (×) were taken from the reference (Zeradjanin, Menzel et al. 2012). The dotted lines were drawn to aid understanding. (b) Raman spectra of ICO, IrO_2, and Co_3O_4 electrodes.

4.3.8. XPS analysis

The repressed OER activity of ICO can be interpreted by the oxidation state of the components in ICO examined by XPS analysis (Figure 4-11). In the XPS spectra regarding Co 2p of ICO and Co_3O_4 (Figure 4-11a), the peaks at 782.9 eV and 798.2 eV are related to Co (II), and the peaks at 781.0 eV and 795.1 eV correspond to Co (III) peaks (Li, Kong et al. 2018, Liu, Bai et al. 2019, Wang, Hao et al. 2020). To compare the oxidation degrees of ICO and Co_3O_4, the ratio of Co (III)/Co (II) was calculated by the areas of respective peaks. The ratio of Co (III)/Co (II) was 1.5 and 1.3 for ICO and Co_3O_4 electrodes, respectively. In other words, Co atoms in ICO are more oxidized than those in pristine Co_3O_4. However, in the Ir 4f spectrum (Figure 4-11b), the ratio of Ir (IV)/Ir (III) of ICO and IrO_2 was 1.7 and 1.5, respectively, which is calculated with the peaks of Ir (III) at 62.4 eV and 65.4 eV and Ir (IV) at 63.2 eV and 66.3 eV (Zhu, Liu et al. 2018, Park, Lee et al. 2020, Liu, Zhang et al. 2021). This implies that Ir species in ICO are less oxidized than those in IrO_2. In short, in ICO, Co atoms are more oxidized and Ir atoms are less oxidized compared to pristine Co_3O_4 and IrO_2. Therefore, in ICO, Co atoms would show better affinity with the partially negatively charged oxygen atoms which is the intermediate during OER, while Ir atoms have less affinity. Considering Co_3O_4 has higher OER overpotential than IrO_2, Co and Ir atoms in ICO changed to an unfavorable state for OER, leading to suppressed OER activity on ICO.

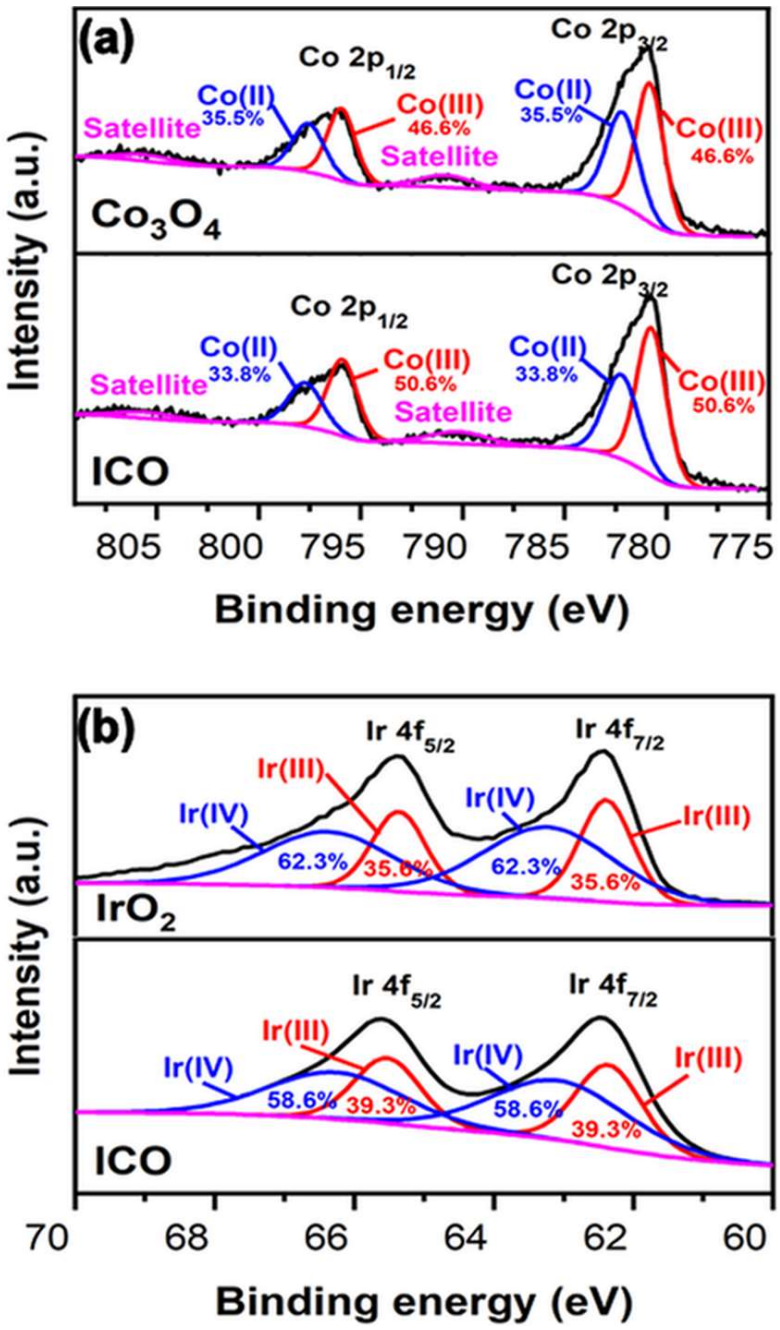

Figure 4-11. XPS spectra of (a) Co 2p of Co_3O_4 and ICO electrodes, and (b) Ir 4f of IrO_2 and ICO electrodes.

4.3.9. The stability of the iridium-cobalt mixed oxide electrode

The anodic stability of ICO, Co_3O_4, and IrO_2 electrodes were tested at 0.1 A cm^{-2} in 0.5 M H_2SO_4 solution. As shown in Figure 4-12a, both ICO and IrO_2 electrodes show notable stability (>200 h), while the Co_3O_4 electrode shows a lifetime of 4h. EDS analysis was conducted after the accelerated stability test (AST), and it was found that the Co atomic ratio of after-AST (34%) only decreases about 12% of the initial state (46%, Table 4-4). In addition, the CER current efficiency of ICO after AST is 14.5%, which is about 1.5 times greater than that of pristine IrO_2 electrode (9.7%) whereas the CER efficiency of IrO_2 after AST is only 7.6% (Figure 4-12b). The higher stability of ICO compared to Co_3O_4 can be explained by the mechanism for the loss of electrocatalytic activity of anode. It has been suggested that anode lost its electrocatalytic activity when Ti substrate is oxidized to form an insulating TiO_2 layer at the substrate coating interface (Ito, Murakami et al. 1996, Yi, Kangning et al. 2007). Therefore, it seems that the Ir content in ICO prevents the oxidation of Ti substrate via its high redox activity.

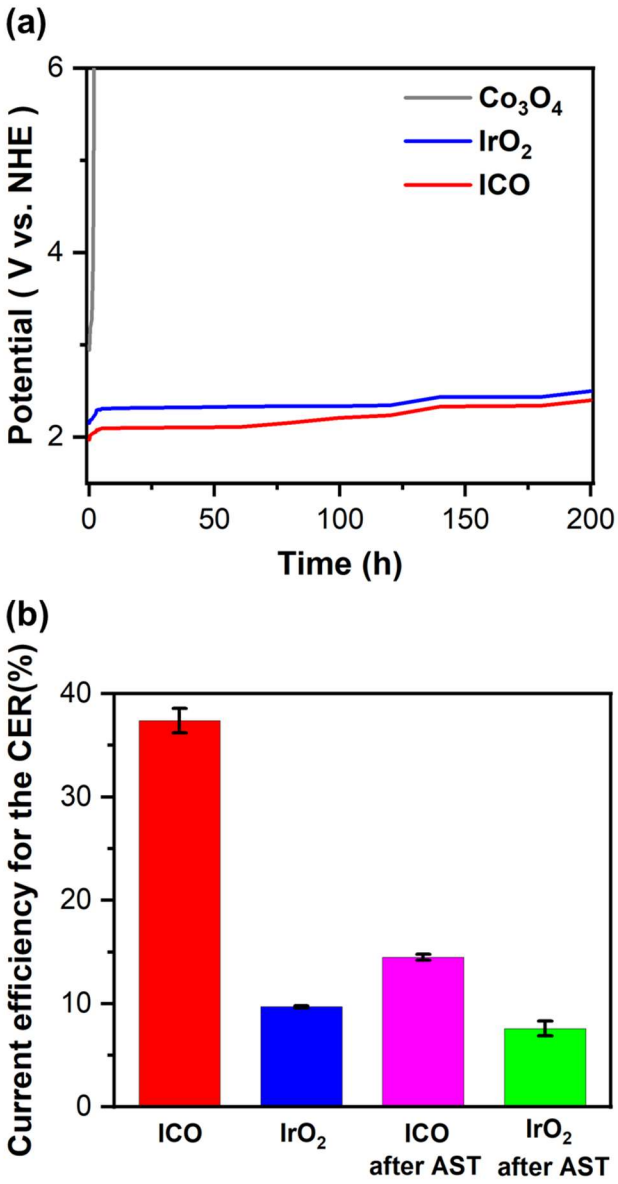

Figure 4-12. (a) Accelerated stability test of ICO, IrO_2, and Co_3O_4 electrodes (0.5 M H_2SO_4, pH 0.3, current density: 0.1 A cm^{-2}). (b) CER current efficiency of ICO and IrO_2 electrodes after accelerated stability test compared to the initial value.

Table 4-4. EDS data of ICO electrode before and after accelerated stability test.

Element	Before AST	After AST
Ir	2	2
Co	46	34
O	52	64

4.3.10. Ammonium degradation

The ICO, Co_3O_4, and IrO_2 electrodes are examined for anodic oxidation of ammonium as a representative contaminant (Figure 4-13). As expected, ICO shows the highest removal efficiency (52.1%) followed by Co_3O_4 (30.6%), and IrO_2 (6.6%) after the 1 h degradation process. The ICO outperforms the Co_3O_4 and IrO_2 due to its higher CER activity in dilute chloride solutions. In addition, the CER by-products such as ClO_2^-, ClO_3^-, and ClO_4^- were not detected by ion chromatography analysis which means by-products were not generated or generated in extremely low concentrations. Therefore, ICO would act as an optimal anode for contaminants degradation in dilute aqueous solutions.

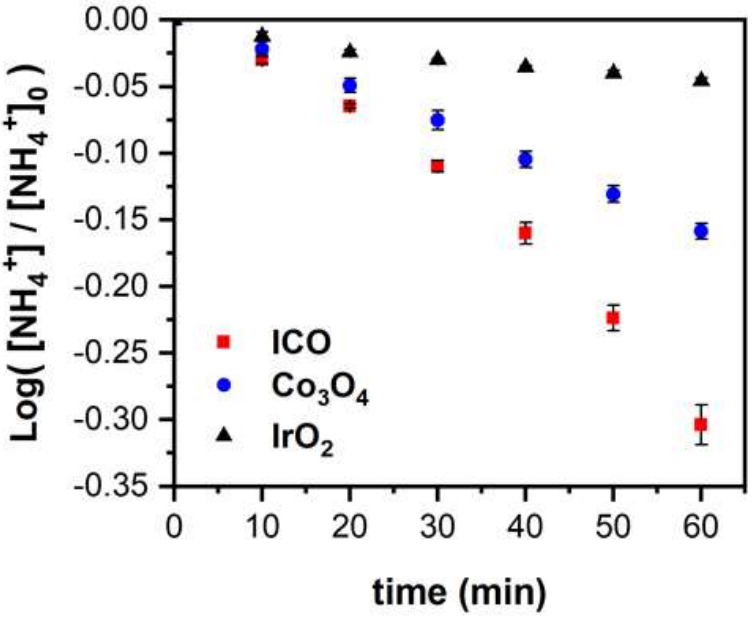

Figure 4-13. NH_4^+ degradation with ICO, IrO_2, and Co_3O_4 electrodes in 2 mM of ammonium with 15mM of chloride solution (current density: 10 mA cm^{-2}).

4.4. Summary

In this study, we reported ICO electrode which showed high CER current efficiency and anodic stability in dilute chloride solutions. The ICO exhibited higher current efficiency for CER with lower energy consumption than IrO_2 not only in dilute solutions but also in concentrated solutions. It is attributed to its low CER overpotential with high OER overpotential. The high CER activity of ICO was demonstrated with high similarity of vibrational frequency between ICO and Cl−O by Raman spectroscopy. Meanwhile, suppressed OER activity of ICO was analyzed with XPS showing more oxidized Co atoms with less oxidized Ir atoms in ICO. The ICO exhibited remarkable stability (> 200 h) in 0.5 M H_2SO_4 solution due to redox-active Ir species. In addition, the ICO outperformed IrO_2 for ammonium degradation in dilute aqueous solutions. Consequently, the ICO could act as an optimal electrocatalytic anode in dilute chloride solutions for its high CER efficiency, low energy consumption, low cost and high anodic stability.

Chapter 5. Conclusions

Due to the severe decrease in the current efficiency for chlorine evolution reaction (CER) of DSAs in dilute chloride solutions, it was necessary to investigate the alternative electrode materials for improving the CER efficiency. Our strategy to enhance the CER efficiency was the adoption of catalysts that can suppress the competitive reaction of CER, namely oxygen evolution reaction (OER). Iron and cobalt were introduced as an OER suppressor because their relatively much higher overpotential of OER compared with that of CER was expected to enhance the CER selectivity. For reliable stability, iridium oxide was mixed with each electrode material.

First, we fabricated the iridium-iron mixed oxide electrode ($0.3IrO_y \cdot 0.7FeO_z$) to enhance the current efficiency for CER in dilute Cl^- solutions. The $0.3IrO_y \cdot 0.7FeO_z$ exhibited far better current efficiency for CER compared with IrO_2 as a representative of DSA, not only in a dilute Cl^- solution but also in a concentrated Cl^- solution. The charge transfer resistance (R_{ct}) of $0.3IrO_y \cdot 0.7FeO_z$ for CER was as fast as that of IrO_2, while R_{ct} for OER was much higher than that of IrO_2. It is attributed to the synergistic effect originating from amphoteric behavior, including FeO_x-like (slow OER rate) and IrO_2-like (fast CER rate) aspects. The $0.3IrO_y \cdot 0.7FeO_z$ also showed reliable stability and safety regarding byproducts

formation. Moreover, the feasibility of $0.3IrO_y \cdot 0.7FeO_z$ for environmental application was successfully proved with arsenite oxidation, ammonium removal, and direct electrolysis of tap water.

Secondly, the iridium-cobalt mixed oxide electrode (ICO) was also fabricated for improving CER current efficiency in dilute chloride solutions. The ICO showed higher CER activity and lower energy consumption than that of the IrO_2 not only in dilute aqueous solutions but also in concentrated solutions. It is attributed to its low CER overpotential with high OER overpotential and low CER charge transfer resistance. The ICO electrode exhibited remarkable stability (> 200 h) in 0.5M H_2SO_4 solution. In addition, the ICO outperformed IrO_2 for ammonium degradation in dilute aqueous solutions. Consequently, the ICO could act as an optimal electrocatalytic anode in dilute chloride solutions for its high CER current efficiency, low energy consumption, low cost and high anodic stability.

The results suggest that $0.3IrO_y \cdot 0.7FeO_z$ and ICO can be a good alternative to DSA and has the potential to expand the application of electrochlorination systems in dilute Cl^- solutions.

References

Braverman, L. E., X. He, S. Pino, M. Cross, B. Magnani, S. H. Lamm, M. B. Kruse, A. Engel, K. S. Crump and J. P. Gibbs (2005). "The effect of perchlorate, thiocyanate, and nitrate on thyroid function in workers exposed to perchlorate long-term." The Journal of Clinical Endocrinology & Metabolism **90**(2): 700-706.

Carroll, G. M. and D. R. Gamelin (2016). "Kinetic analysis of photoelectrochemical water oxidation by mesostructured Co-Pi/α-Fe2O3 photoanodes." Journal of Materials Chemistry A **4**(8): 2986-2994.

Choi, J., S. Shim and J. Yoon (2013). "Design and operating parameters affecting an electrochlorination system." Journal of Industrial and Engineering Chemistry **19**(1): 215-219.

Cong, Y., M. Chen, T. Xu, Y. Zhang and Q. Wang (2014). "Tantalum and aluminum co-doped iron oxide as a robust photocatalyst for water oxidation." Applied Catalysis B: Environmental **147**: 733-740.

Cotillas, S., J. Llanos, M. A. Rodrigo and P. Canizares (2015). "Use of carbon felt cathodes for the electrochemical reclamation of urban treated wastewaters." Applied Catalysis B: Environmental **162**: 252-259.

Czarnetzki, L. and L. Janssen (1992). "Formation of hypochlorite, chlorate and oxygen during NaCl electrolysis from alkaline solutions at an RuO2/TiO2 anode." Journal of Applied Electrochemistry **22**(4): 315-324.

Da Silva, L. M., J. Boodts and L. A. De Faria (2001). "Oxygen evolution at RuO2 (x)+Co3O4(1−x) electrodes from acid solution." Electrochimica Acta **46**(9): 1369-1375.

De Faria, L., J. Boodts and S. Trasatti (1996). "Electrocatalytic properties of ternary oxide mixtures of composition Ru 0.3 Ti (0.7−x) CexO2: oxygen evolution from acidic solution." Journal of applied electrochemistry **26**(11): 1195-1199.

Du, Q., S. Zhang, B. Pan, L. Lv, W. Zhang and Q. Zhang (2013). "Bifunctional resin-ZVI composites for effective removal of arsenite through simultaneous adsorption and oxidation." Water research **47**(16): 6064-6074.

Fontenot, S., S. Lee and K. Asche (2013). "The effects of chloride from waste water on the environment." Center for Small Towns. http://environment. umn. edu/wpcontent/uploads/2016/03/MS-0008-12-Final-Addendum. pdf (last accessed 4 May 2019).

Fu, Z., T. Jiang, L. Zhang, B. Liu, D. Wang, L. Wang and T. Xie (2014). "Surface treatment with Al 3+ on a Ti-doped α-Fe2O3 nanorod array photoanode for efficient photoelectrochemical water splitting." Journal of Materials Chemistry A **2**(33): 13705-13712.

Gokuladeepan, P. and A. Karthigeyan (2018). "Effect of annealing temperature on oxygen reduction reaction of reduced graphene oxide incorporated cobalt oxide nanocomposites for fuel cell applications." Applied Surface Science **449**: 705-711.

Goldfrank, L. R., R. S. Hoffman, M. A. Howland and N. A. Lewin (2006).

Goldfrank's toxicologic emergencies, McGraw Hill Professional.

Grgur, B. N. and D. Ž. Mijin (2014). "A kinetics study of the methomyl electrochemical degradation in the chloride containing solutions." Applied Catalysis B: Environmental **147**: 429-438.

Han, H., I. Kim and S. Park (2020). "Cobalt-based oxygen evolution catalyst as active and stable as iridium in acidic media." Electrochimica Acta **344**: 136160.

Hansen, H. A., I. C. Man, F. Studt, F. Abild-Pedersen, T. Bligaard and J. Rossmeisl (2010). "Electrochemical chlorine evolution at rutile oxide (110) surfaces." Physical Chemistry Chemical Physics **12**(1): 283-290.

Hong, C. C., S.-K. Chan and H. Shim (2007). "Effect of chloride on biological nutrient removal from wastewater." Journal of Applied Sciences in Environmental Sanitation **2**(3): 85-92.

Hong, S., T.-k. Lee, M. R. Hoffmann and K. Cho (2020). "Enhanced chlorine evolution from dimensionally stable anode by heterojunction with Ti and Bi based mixed metal oxide layers prepared from nanoparticle slurry." Journal of Catalysis **389**: 1-8.

Hooper, J. (2005). ON-SITE GENERATION OF SODIUM HYPOCHLORITE BASIC OPERATING PRINCIPLES AND DESIGN CONSIDERATIONS. Annual Water Industry Engineers and Operators Conference.

Hu, J.-M., J.-Q. Zhang and C.-N. Cao (2004). "Oxygen evolution reaction on IrO2-based DSA® type electrodes: kinetics analysis of Tafel lines and EIS." International

Journal of Hydrogen Energy **29**(8): 791-797.

Hummelgård, C., R. K. Karlsson, J. Bäckström, S. M. Rahman, A. Cornell, S. Eriksson and H. Olin (2013). "Physical and electrochemical properties of cobalt doped (Ti, Ru) O2 electrode coatings." Materials Science and Engineering: B **178**(20): 1515-1522.

Ito, M., Y. Murakami, H. Kaji, K. Yahikozawa and Y. Takasu (1996). "Surface characterization of RuO2-SnO2 coated titanium electrodes." Journal of the Electrochemical Society **143**(1): 32.

Jeong, J., J. Y. Kim, M. Cho, W. Choi and J. Yoon (2007). "Inactivation of Escherichia coli in the electrochemical disinfection process using a Pt anode." Chemosphere **67**(4): 652-659.

Kartinen Jr, E. O. and C. J. Martin (1995). "An overview of arsenic removal processes." Desalination **103**(1-2): 79-88.

Khelifa, A., S. Aoudj, S. Moulay and M. De Petris-Wery (2013). "A one-step electrochlorination/electroflotation process for the treatment of heavy metals wastewater in presence of EDTA." Chemical Engineering and Processing: Process Intensification **70**: 110-116.

Khelifa, A., S. Moulay, F. Hannane, S. Benslimene and M. Hecini (2004). "Application of an experimental design method to study the performance of electrochlorination cells." Desalination **160**(1): 91-98.

Kim, J., C. Kim, S. Kim and J. Yoon (2015). "A Review of Chlorine Evolution

Mechanism on Dimensionally Stable Anode (DSA®)." Korean Chemical Engineering Research **53**(5): 531-539.

Kraft, A., M. Stadelmann, M. Blaschke, D. Kreysig, B. Sandt, F. Schröder and J. Rennau (1999). "Electrochemical water disinfection Part I: Hypochlorite production from very dilute chloride solutions." Journal of Applied Electrochemistry **29**(7): 859-866.

Lacasa, E., P. Cañizares, M. A. Rodrigo and F. J. Fernández (2012). "Electro-oxidation of As (III) with dimensionally-stable and conductive-diamond anodes." Journal of hazardous materials **203**: 22-28.

Lakshmipathiraj, P., S. Prabhakar and G. B. Raju (2010). "Studies on the electrochemical decontamination of wastewater containing arsenic." Separation and Purification Technology **73**(2): 114-121.

Le Luu, T., J. Kim and J. Yoon (2015). "Physicochemical properties of RuO2 and IrO2 electrodes affecting chlorine evolutions." Journal of Industrial and Engineering Chemistry **21**: 400-404.

Li, J., X. Kong, M. Jiang and X. Lei (2018). "Uniformly dispersed Pd nanoparticles anchored Co(OH)2/Cu(OH)2 hierarchical nanotube array as high active structured catalyst for Suzuki–Miyaura coupling reactions." Journal of Materials Science **53**(24): 16263-16275.

Liu, C., G. Bai, X. Tong, Y. Wang, B. Lv, N. Yang and X.-Y. Guo (2019). "Mesoporous and ultrathin arrays of cobalt nitride nanosheets for electrocatalytic

oxygen evolution." Electrochemistry Communications **98**: 87-91.

Liu, F., L. Zhang, L. Wang and F. Cheng (2021). "The Electrochemical Tuning of Transition Metal-Based Materials for Electrocatalysis." Electrochemical Energy Reviews: 1-23.

Malpass, G., D. Miwa, D. Mortari, S. Machado and A. Motheo (2007). "Decolorisation of real textile waste using electrochemical techniques: effect of the chloride concentration." Water research **41**(13): 2969-2977.

Mendia, L. (1982). "Electrochemical processes for wastewater treatment." Water Science and Technology **14**(1-2): 331-344.

Menzel, N., E. Ortel, K. Mette, R. Kraehnert and P. Strasser (2013). "Dimensionally stable Ru/Ir/TiO2-anodes with tailored mesoporosity for efficient electrochemical chlorine evolution." Acs Catalysis **3**(6): 1324-1333.

Moser, M., C. Mondelli, A. P. Amrute, A. Tazawa, D. Teschner, M. E. Schuster, A. Klein-Hoffman, N. r. López, T. Schmidt and J. Pérez-Ramírez (2013). "HCl oxidation on IrO2-based catalysts: from fundamentals to scale-up." ACS Catalysis **3**(12): 2813-2822.

Nath, H., X. Wang, R. Torrens and A. Langdon (2011). "A novel perforated electrode flow through cell design for chlorine generation." Journal of Applied Electrochemistry **41**(4): 389-395.

Neodo, S., D. Rosestolato, S. Ferro and A. De Battisti (2012). "On the electrolysis of dilute chloride solutions: Influence of the electrode material on Faradaic

efficiency for active chlorine, chlorate and perchlorate." Electrochimica Acta **80**: 282-291.

Oakton, E., D. Lebedev, M. Povia, D. F. Abbott, E. Fabbri, A. Fedorov, M. Nachtegaal, C. Copéret and T. J. Schmidt (2017). "IrO2-TiO2: A high-surface-area, active, and stable electrocatalyst for the oxygen evolution reaction." ACS Catalysis **7**(4): 2346-2352.

Panić, V., A. Dekanski, S. Milonjić, R. Atanasoski and B. Nikolić (2000). "The influence of the aging time of RuO2 and TiO2 sols on the electrochemical properties and behavior for the chlorine evolution reaction of activated titanium anodes obtained by the sol-gel procedure." Electrochimica Acta **46**(2-3): 415-421.

Park, Y. J., J. Lee, Y. S. Park, J. Yang, M. J. Jang, J. Jeong, S. Choe, J. W. Lee, J.-D. Kwon and S. M. Choi (2020). "Electrodeposition of high-surface-area IrO2 films on Ti felt as an efficient catalyst for the oxygen evolution reaction." Frontiers in chemistry **8**.

Patermarakis, G. and E. Fountoukidis (1990). "Disinfection of water by electrochemical treatment." Water research **24**(12): 1491-1496.

Rahman, G. and O.-S. Joo (2012). "Photoelectrochemical water splitting at nanostructured α-Fe2O3 electrodes." international journal of hydrogen energy **37**(19): 13989-13997.

Saha, J. and S. K. Gupta (2017). "Endeavor toward competitive electrochlorination by comparing the performance of easily affordable carbon electrodes with

platinum." Chemical Engineering Communications **204**(12): 1357-1368.

Sivula, K., F. Le Formal and M. Grätzel (2011). "Solar water splitting: progress using hematite (α-Fe2O3) photoelectrodes." ChemSusChem **4**(4): 432-449.

Sohrabnejad-Eskan, I., A. Goryachev, K. S. Exner, L. A. Kibler, E. J. Hensen, J. P. Hofmann and H. Over (2017). "Temperature-dependent kinetic studies of the chlorine evolution reaction over RuO2 (110) model electrodes." ACS Catalysis **7**(4): 2403-2411.

Sorlini, S. and F. Gialdini (2010). "Conventional oxidation treatments for the removal of arsenic with chlorine dioxide, hypochlorite, potassium permanganate and monochloramine." Water Research **44**(19): 5653-5659.

Spray, R. L., K. J. McDonald and K.-S. Choi (2011). "Enhancing photoresponse of nanoparticulate α-Fe2O3 electrodes by surface composition tuning." The Journal of Physical Chemistry C **115**(8): 3497-3506.

Tamirat, A. G., W.-N. Su, A. A. Dubale, H.-M. Chen and B.-J. Hwang (2015). "Photoelectrochemical water splitting at low applied potential using a NiOOH coated codoped (Sn, Zr) α-Fe2O3 photoanode." Journal of Materials Chemistry A **3**(11): 5949-5961.

Tavakkoli, M., T. Kallio, O. Reynaud, A. G. Nasibulin, J. Sainio, H. Jiang, E. I. Kauppinen and K. Laasonen (2016). "Maghemite nanoparticles decorated on carbon nanotubes as efficient electrocatalysts for the oxygen evolution reaction." Journal of Materials Chemistry A **4**(14): 5216-5222.

Trasatti, S. (1984). "Electrocatalysis in the anodic evolution of oxygen and chlorine." Electrochimica Acta **29**(11): 1503-1512.

Trasatti, S. (2000). "Electrocatalysis: understanding the success of DSA®." Electrochimica Acta **45**(15-16): 2377-2385.

Tsang, S., F. Phu, M. M. Baum and G. A. Poskrebyshev (2007). "Determination of phosphate/arsenate by a modified molybdenum blue method and reduction of arsenate by S2O42−." Talanta **71**(4): 1560-1568.

Vos, J. G., Z. Liu, F. D. Speck, N. Perini, W. Fu, S. Cherevko and M. T. Koper (2019). "Selectivity trends between oxygen evolution and chlorine evolution on iridium-based double perovskites in acidic media." ACS catalysis **9**(9): 8561-8574.

Wang, Y., J. Hao, W. Li, X. Zuo, B. Xiang, Y. Qiang, X. Zou, B. Tan, Q. Hu and F. Chen (2020). "Mn 3 O 4/Co (OH) 2 cactus-type nanoarrays for high-energy-density asymmetric supercapacitors." Journal of Materials Science **55**(2): 724-737.

Yang, T.-Y., H.-Y. Kang, K. Jin, S. Park, J.-H. Lee, U. Sim, H.-Y. Jeong, Y.-C. Joo and K. T. Nam (2014). "An iron oxide photoanode with hierarchical nanostructure for efficient water oxidation." Journal of Materials Chemistry A **2**(7): 2297-2305.

Yi, Z., C. Kangning, W. Wei, J. Wang and S. Lee (2007). "Effect of IrO2 loading on RuO2–IrO2–TiO2 anodes: A study of microstructure and working life for the chlorine evolution reaction." Ceramics International **33**(6): 1087-1091.

Yoon, Y., E. Cho, Y. Jung, M. Kwon, J. Yoon and J.-W. Kang (2015). "Evaluation of the formation of oxidants and by-products using Pt/Ti, RuO2/Ti, and IrO2/Ti

electrodes in the electrochemical process." Environmental technology **36**(3): 317-326.

Zeng, Q., J. Bai, J. Li, L. Xia, K. Huang, X. Li and B. Zhou (2015). "A novel in situ preparation method for nanostructured α-Fe2O3 films from electrodeposited Fe films for efficient photoelectrocatalytic water splitting and the degradation of organic pollutants." Journal of Materials Chemistry A **3**(8): 4345-4353.

Zeradjanin, A. R., N. Menzel, P. Strasser and W. Schuhmann (2012). "Role of Water in the Chlorine Evolution Reaction at RuO2-Based Electrodes—Understanding Electrocatalysis as a Resonance Phenomenon." ChemSusChem **5**(10): 1897-1904.

Zhu, Z., X. Liu, Z. Ye, J. Zhang, F. Cao and J. Zhang (2018). "A fabrication of iridium oxide film pH micro-sensor on Pt ultramicroelectrode and its application on in-situ pH distribution of 316L stainless steel corrosion at open circuit potential." Sensors and Actuators B: Chemical **255**: 1974-1982.

국문 초록

본 연구에서는 산소발생반응을 억제할 수 있는 촉매를 이용하여 저농도 Cl^- 용액에서도 효율적으로 염소를 발생시킬 수 있는 전극을 개발하였다. Dimensionally stable anode (DSA; IrO_2, RuO_2)는 염소발생성능과 안정성이 뛰어난 전극으로 알려져 있지만, DSA는 저농도 Cl^-용액에서 염소발생효율이 급격하게 떨어지는 단점이 있다. 이는 DSA의 촉매적 특성에 기인한 것으로, 염소발생반응의 경쟁반응인 산소발생반응도 매우 빠르게 일어나기 때문이다. 이로 인해, 원수의 Cl^-농도에 따라 염소발생시스템의 사용이 매우 제한되거나, 염소발생장치에 높은 Cl^-농도를 지속적으로 유지시켜주기 위한 부가장치들이 필요하다. 따라서 저농도 Cl^-용액에서도 효율적으로 염소를 발생시킬 수 있는 전극개발이 필요하다.

본 연구에서는 산화철과 산화코발트를 산소발생억제 촉매로 도입하여 염소발생효율을 향상시키고자 하였다. 산화철은 주로 산소발생용 전극으로 사용되는 물질로, 다양한 장점이 있지만 산소발생속도가 느리다는 단점이 있다. 산화철의 단점이라고 여겨지던 느린 산소발생속도는 염소발생반응의 관점에서 보면 경쟁반응을 억제시켜 염소발생효율을 향상시킬 수 있는 장점이 될 수 있다. 또한 산화철은 다른 전극물질에 비해 산소발생 과전압이 염소발생 과전압보다 매우 높은 특성이 있어 염소발생 선택도를 향상시켜 줄 수 있다. 이와 비슷하게 산화코발트는 산화철보다 산소발생 과전압은 낮지만, 산소발생과전

압과 염소발생과전압의 차이는 산화철보다 크기 때문에 산화코발트 또한 염소발생효율을 향상시킬 수 있다. 한편, 전위금속을 통한 전극 개발은 꾸준히 이루어졌는데, 해당 전극들은 전극 수명이 너무 짧다는 단점이 있다. 전극의 안정성 향상을 위하여 소량의 IrO_2를 산화철과 산화코발트에 각각 혼합하여 복합전극인 $IrO_y \cdot FeO_z$와 $IrO_a \cdot CoO_b$를 열분해법을 통하여 제조하였다. 다양한 농도 (1 mM – 2000 mM)의 Cl^-용액에서 염소발생실험을 진행한 결과, 해당 전극들은 기존 DSA전극보다 월등히 향상된 염소발생효율을 보였다. 또한 복합전극들의 안정성은 산화철, 산화코발트 전극보다 크게 향상되었고, ClO_2^-, ClO_3^-, ClO_4^- 와 같은 부산물 생성도 먹는물 기준 이하로 검출되었다. 복합전극인 $IrO_y \cdot FeO_z$와 $IrO_a \cdot CoO_b$ 전극의 향상된 염소발생특성은 산화철, 산화코발트 성분의 산소발생 억제특성과 IrO_2 성분의 빠른 염소발생특성에 기인한다.

위 결과들을 종합하여 볼 때, $IrO_y \cdot FeO_z$와 $IrO_a \cdot CoO_b$ 전극은 원수의 조성에 상관없이 염소를 효율적으로 발생시킬 수 있는 전극으로 전기화학적 염소발생 시스템의 적용범위를 현저하게 넓힐 수 있을 것으로 기대된다.

주요어: 산화철; 산화코발트; 염소발생반응; 산소발생반응; 전기화학적 염소주입법

학번: 2017-33653